A non-peer reviewed preprint submitted to EarthArXiv

Towards Prospective Disaster Risk Management: Mapping Multi-hazard Urban Risk Dynamics Driven by Evolving Exposure & Vulnerability via Earth Observation

Joshua Dimasaka[1,2,3*]
Fouad Bendimerad[3], Renan Ma. Tanhueco[3,4], Christian Geiß[5,6], Emily So[1,2]

[1*]Department of Architecture, University of Cambridge, United Kingdom.
[2]Cambridge University Centre for Risk in the Built Environment, United Kingdom.
[3]Earthquakes and Megacities Initiative, Philippines.
[4]Department of Civil Engineering, De La Salle University, Philippines.
[5]Earth Observation Center, German Aerospace Center, Germany.
[6]Institute of Geography, University of Bonn, Germany.

*Corresponding author(s). E-mail(s): jtd33@cantab.ac.uk;

Abstract

As local governments increasingly adopt geospatial Climate and Disaster Risk Assessment (CDRA) to inform prospective public policy, the reliability of existing static risk intelligence is challenged by the continuous evolution of building exposure, population distribution, and physical vulnerability. Recent multi-temporal datasets of the built environment, derived from Earth Observation and volunteered geographic information, have enabled comprehensive regional exposure-hazard analyses. However, their intersection with physical vulnerability remains underexplored to translate into risk dynamics at the neighbourhood-to-city scale. To investigate the utility of high-resolution multi-temporal building height data from the Google Open Buildings 2.5D Temporal dataset and publicly available Copernicus Sentinel-2 imagery for projecting exposure and vulnerability through probabilistic graph deep learning, we evaluated the multi-hazard urban risk dynamics under the compounding effects of earthquake and flood in Quezon City, Philippines, as a case study. We derived annual development profiles in built-up area, building materials (wood, masonry, concrete, and steel), damaged floor area, casualty estimates, and multi-hazard displacement spanning 2016–2030, while emphasising key uncertainties in regional exposure and vulnerability modelling that remain challenging in practice. Variability in growth trajectories across 142 neighbourhoods (locally known as barangays) reflects disparities in the affordability of building materials and identifies strategic hotspots for housing retrofit programmes and healthcare demand planning. A comparison against the existing geospatial exposure database further reveals opportunities to advance the current state of practice in building stock attribution. In conclusion, rapidly urbanising cities such as Quezon City have experienced uneven trajectories of multi-hazard risk across neighbourhoods in recent years, underscoring the need for sustained scientific scrutiny and rigorous validation of CDRA to support effective prospective disaster risk management at scale.

Keywords: spatiotemporal, multi-hazard, prospective risk, spatiotemporal, exposure, physical vulnerability, cities, neighbourhood

JEL Classification: O15 , O18 , O20 , Q54 , Q56 , R11 , R14 , R31 , C53 , C55 , D81 , O33 , C45

MSC Classification: 68T07 , 68T09 , 62H35 , 60G60 , 62M30 , 62P12 , 86A32 , 91B76 , 90B15

1 Introduction

In the increasing adoption of digital mapping technologies in many local governments, the geospatial knowledge on Climate and Disaster Risk Assessment (CDRA) has become the scientific backbone that directly underpins many critical public policy instruments (Amaratunga et al. 2019; Costa et al. 2024), such as comprehensive land use plans (Lagmay et al. 2024), emergency management (Freire et al. 2013), healthcare resource management (Hou et al. 2023), risk transfer financing mechanisms (Cabi et al. 2021), and recovery aid allocation (Loos et al. 2020). However, as the scale of climatic hazard intensifies and cascades, coupled with the accelerating urbanisation, such risk intelligence is rapidly becoming outdated from using static exposure database of physical assets in the form of fixed building stock inventories with varying levels of uncertainty (Schorlemmer et al. 2026; Huyck et al. 2022).

Amidst the institutional barriers and challenges in local capacity development (Malalgoda et al. 2016), this raises a critical question on how frequently local governments should update, fund, and re-conduct their geospatial risk assessments to ensure that their public policies remain relevant to the increasing exposure of the growing vulnerable population. As public policies are more regularly updated with fiscal appropriation of local governments, the reliability against under- and over-estimation of disaggregated risk information due to temporally inadequate data directly shapes the sustainable and equitable reduction and management of climate and disaster risk at the community level. Beyond improving the accuracy of exposure information with the most updated characterisation, tracking the trajectory of historical changes in geospatial risk information can pinpoint areas that need targeted and localised solutions towards prospective disaster risk management at scale.

The United Nations Office for Disaster Risk Reduction (UNDRR) (2017) defines prospective disaster risk management (PDRM) as a set of activities that ”address and seek to avoid the development of new or increased disaster risks.” In their recent Global Assessment Report on Disaster Risk Reduction (GAR) (UNDRR 2025a) and Strategic Framework 2026-2030 (UNDRR 2025b), the future-oriented decision-making aspect of PDRM can involve the use of tools such as probabilistic hazard models with metrics like average annual loss (AAL) and probable maximal loss (PML) or through the integration of demographic and urban growth projections for enhancing exposure and vulnerability data. While the use of AAL and PML from probabilistic hazard models is suitable for pricing catastrophe insurance policies for individual housing market or shared economy-wide entities like risk pools among cities and countries (Gignac-Eddy et al. 2020), the technical and fiscal capacity of many local governments at the scale of neighbourhoods are however more appropriately positioned to public policies on emergency preparedness and post-disaster recovery, which rather rely on the deterministic- or scenario-based hazard maps, instead of its probabilistic equivalents (McGuire 2001). Several studies have also shown that local governments play a key role on the frontlines with significant social ties to their communities and local knowledge (Basu et al. 2013).

Following this context, how the projections on demography and urban growth influence the spatiotemporal distribution of exposure and vulnerability can provide the basis for developing local PDRM plans. Several studies have shown how this can inform (1) urban planning policies in the cities of Hanoi (Vietnam), Nagoya (Japan), Shanghai (China), and Hartford (United States) (Pham et al. 2011); (2) future multi-hazard risk management in Vancouver (Canada) (Chang et al. 2019); and (3) people-centred decision-making for post-disaster financial assistance programs and building code compliance in Istanbul (Türkiye), Nablus (Palestine), Chattogram (Bangladesh), Cox’s Bazaar (Bangladesh), Nairobi (Kenya), Nakuru (Kenya), Quito (Ecuador), Kokhana (Nepal), Rapti (Nepal) and Darussalam (Tanzania) (Cremen et al. 2022, 2023, 2026). However, as a demonstrated case study in this work, while the Philippine government mandates the development of a Comprehensive Land Use Plan (CLUP) from which CDRA becomes vital (HLURB 2013), current CDRA in practice (EMI 2022) remains limited to fixed building stock inventories and other exposure indicators such as population, although climate projections have already been integrated (HLURB 2015). Limited to hazard-based alone, this shortcoming, undermining local PDRM capability, is primarily dictated by the lack of available and validated temporal data on fine-grained projections at the community level, in addition to its inherently expensive data collection and monitoring requirements. Consequently, this reflects a policy gap yet an ample opportunity in mainstreaming PDRM across all elements of climate and disaster risk, not only about intensifying hazard but also under evolving exposure and vulnerability, for effective design of sustainable long-term community resilience.

The increasing availability of global multi-temporal datasets from Earth Observation and volunteered geographic information systems (Woods et al. 2025; Sirko et al. 2021, 2023; Glazer et al. 2025; Pesaresi et al. 2024; Marconcini et al. 2021) has enabled a growing body of research on the dynamics of evolving exposure and vulnerability patterns under the compounding and cascading effects of multiple hazards. Drawing on these datasets, recent studies have investigated the spatiotemporal intersections of built-up expansion, population growth, and hazard intensification across a range of contexts and scales. Stalhandske et al. (2025) documented a 69% global increase in per capita exposure to three or more hazards, including heatwaves, droughts, wildfires, extreme precipitation, river floods, and tropical cyclones, between 2003 and 2021 using the WorldPop population dataset at 0.25-degree resolution. Wang et al. (2026) demonstrated increasing exposure of human settlements to landslide susceptibility elevated by intensified rainfall patterns from 2000 to 2025 using Global Human Settlement Layer products at 0.1-degree resolution. Rentschler et al. (2023) revealed rapid global urbanisation within flood zones since 1985 using DLR World Settlement Footprint data at 30-m resolution. At the city scale, Xia et al. (2026) identified three distinct developmental stages in the dryland expansion of Windhoek, Namibia, through the relationship between informal settlement growth and land surface temperature using the Google Open Buildings 2.5D Temporal dataset and Landsat imagery at 50-cm and 30-m resolution, respectively, while Lee and Kim (2026) analysed daytime and nighttime population exposure under compounding earthquake-flood scenarios (Quigley and Duffy 2020) in Seoul, South Korea, at 250-m resolution. Despite the valuable insights into multi-hazard urbanisation dynamics, their focus on the spatiotemporal intersection of exposure and hazard alone does not translate into risk-informed understanding yet, without the underexplored role of physical vulnerability across the varying scales from global to community level.

Our Contribution. Therefore, our work demonstrates multi-hazard urban risk dynamics driven by both evolving exposure and vulnerability derived from Earth observation data through probabilistic graph deep learning (Dimasaka et al. 2026b) using the case study of Quezon City (Philippines). At the neighbourhood-to-city scale, we provide a significant extension to its previous regional risk assessment of Quezon City (EMI 2022; Dimasaka 2022; Allen et al. 2014) with about 3 million population in 142 administering neighbourhoods (hereafter, *barangay* or *brgy*) exposed to both magnitude-7.2 West Valley Fault earthquake scenario and recurring flooding events comparable to RCP8.5 100-year return period. Complementing the absolute measures of earthquake and flood risk, our work generates maps of annual development profiles of building exposure and population, building material of physical vulnerability, earthquake risk by building damage state and casualty, and multi-hazard displacement, thereby providing the local government of Quezon City with relevant risk-informed insights for developing their local forward-looking PDRM plans. Our integration of the Google Open Buildings 2.5D Temporal dataset also presents improvements in the existing static geospatial exposure database.

The remainder of this paper is organised as follows: Section 2 describes the geography and risk profile of Quezon City, including the datasets across the three elements of risk: multi-temporal high-resolution building exposure, prior physical vulnerability, and multi-hazard scenarios.

Section 3 provides an overview of the implementation of probabilistic graph deep learning, a data-driven model of exposure and vulnerability, and then presents the assessment of earthquake and flood risk. Section 4 discusses the derived maps of annual development profiles, followed by the reported improvements on the existing exposure database and benchmarking with the most recent CDRA of Quezon City. Section 5 enumerates various methodological limitations as opportunities that can be further addressed in future work.

2 Materials

2.1 Study Area: Quezon City, Philippines

With a land mass of about 161 km^2, Quezon City in the northeast portion of Metro Manila has the largest population of over 2.9 million (as of 2015) among all 33 highly urbanised cities in the Philippines, occupying over one-fourth of the size of the metropolitan (QCPDO 2022). The city comprises six districts (numbered 1-6) with 37, 5, 37, 38, 14, and 11 barangays, respectively, as shown in Figure 1, Figure 2, and Figure 3. Over the years, the city has urbanised with about 30% residential with a ribbon-type commercial development concentrated around major transportation networks. Despite the growing demography of predominantly young at a median age of 27, the QCPDO (2022) further reported that, in 2022, about 209,350 families still lived in informal settlements, and, in 2021, the poverty incidence rate (among population) is at 3.0%, which is equivalent to 94,134 residents with insufficient income for minimum basic needs. This critical background information is important in the context of our work that examines the growth in multi-hazard displacement, exacerbating these existing socio-economic conditions of the city.

2.2 Multi-temporal High-resolution Building Exposure

The exposure dataset of Quezon City has undergone multiple refinements over two decades, evolving from the foundational Metro Manila Earthquake Impact Reduction Study (MMEIRS) in 2002 to 2004. This improved in the 2006 Air Quality Study by the Metropolitan Manila Development Authority (MMDA) and subsequently by the 2014 Greater Metro Manila Area Risk Analysis Project (GMMA-RAP), the first megacity multi-hazard risk assessment to integrate time-series Landsat multi-spectral and aerial imagery, digital elevation and surface models at 1-m resolution, 2010 census data on population and housing, and other remote sensing information (Bautista et al. 2014). Despite extensive field survey validation, Bautista et al. (2014) recognised several modelling challenges, including cloud corruption and lighting illumination artefacts in satellite imagery, false negatives in building detection where rooftops were spectrally similar to vegetation or non-structural accessories such as covered walkways, uncertainty in inter-storey heights by occupancy type, incomplete census information for select barangays, and inherent model uncertainties from unsupervised land use classification. In 2022, the Earthquakes and Megacities Initiative (EMI) performed a significant update through manual digitisation using the latest digital elevation and surface models and high-resolution orthoimagery at about 0.40-m resolution (EMI 2022). These successive updates both reflect the growing interest in city exposure modelling in practice and the methodological challenges that motivate the probabilistic and data-driven approach adopted in this work.

Building on these developments, this work leverages the publicly available high-resolution 50-cm annual building height data from the Google Open Buildings 2.5D Temporal dataset (2016 to 2021), derived from Copernicus Sentinel-2 imagery through a super-resolution technique with a mean absolute error of 1.5 m and a coefficient of determination, R^2, of 0.91 (Sirko et al. 2023). Recognising that building height data alone provides insufficient discriminative power for material typology classification to support the probabilistic graph deep learning, we incorporated additional physically interpretable covariates from Copernicus Sentinel-2 imagery, including multi-spectral bands and other derived spectral indices (Dimasaka et al. 2026b).

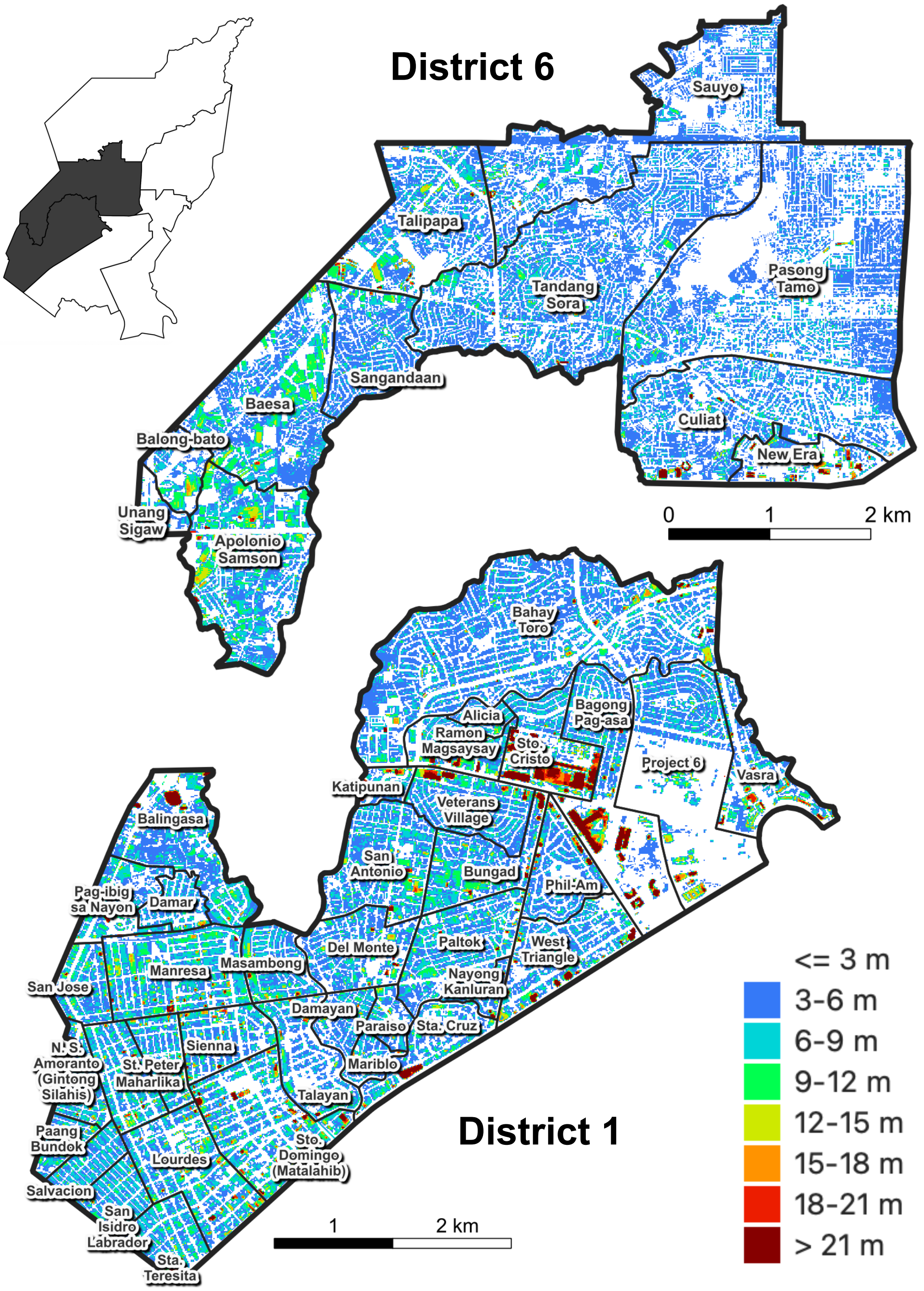

Figure 1: The administrative boundaries of barangays in Districts 1 and 6 (EMI 2022) showing our derived 2020 building height data at 10-m resolution.

Hence, we resampled these building height maps at 50-cm resolution into coarser 10-m grids and expressed the building height ($\mathbf{E_{BH}}$) within each grid using the non-negative constraint (i.e., $\mathbf{E_{BH}} \geq 0$) of the lognormal probability distribution as:

$$\ln \mathbf{E_{BH}} \sim \mathcal{N}(\boldsymbol{\mu}, \boldsymbol{\Sigma}) \tag{1}$$

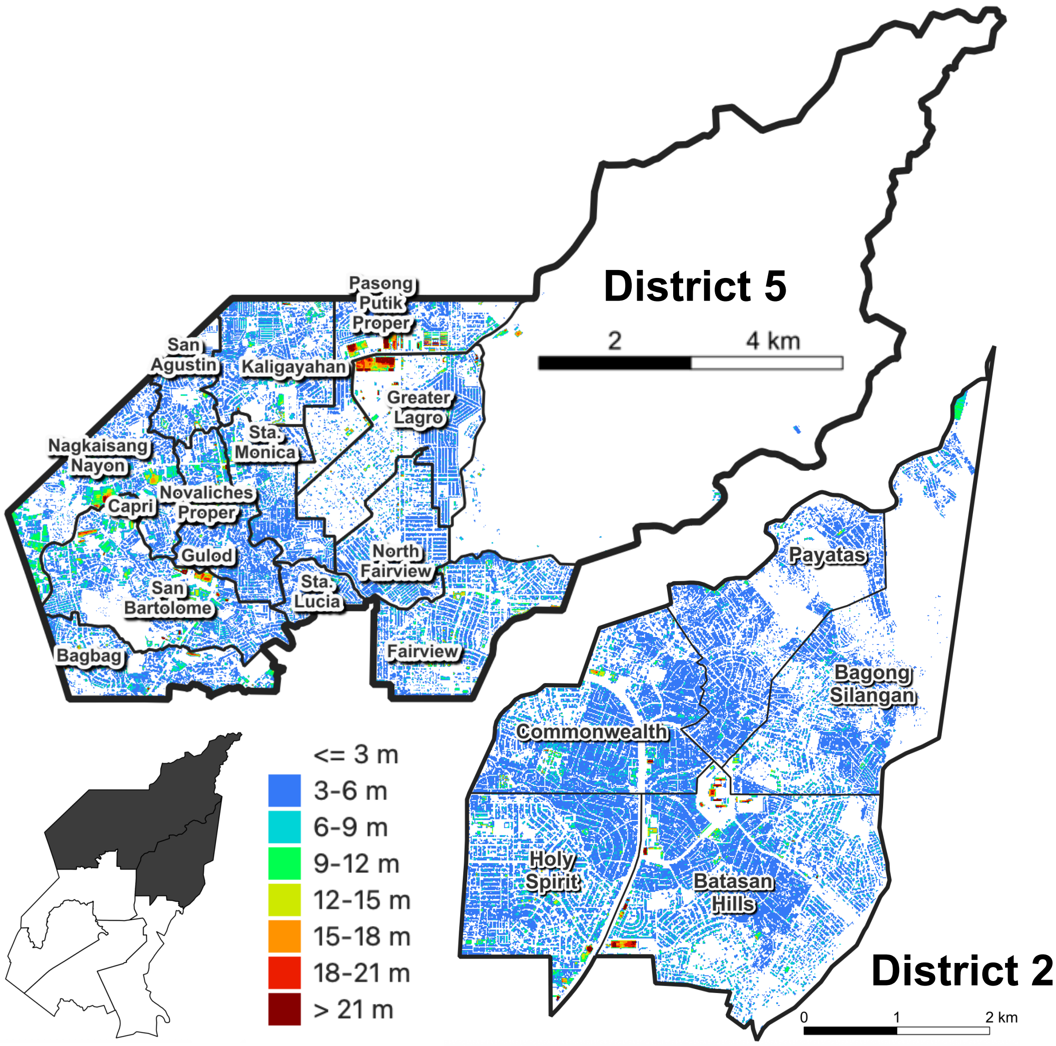

Figure 2: The administrative boundaries of barangays in Districts 2 and 5 (EMI 2022) showing our derived 2020 building height data at 10-m resolution.

where $\boldsymbol{\mu}$ and $\boldsymbol{\Sigma}$ are the mean and variance of fine-grained building height values at 50-cm resolution within each 10-m grid. The resulting 2016-2021 maps serve as prior distributions for building heights, which are inputs to our graph-based deep neural network with parameters $\boldsymbol{\theta}$ that transform the prior parameters $(\boldsymbol{\mu}, \boldsymbol{\Sigma})$ into posterior estimates $(\boldsymbol{\mu}_\theta, \boldsymbol{\Sigma}_\theta)$, enabling projections for the period from 2022 to 2030, as shown in Figure 4. To illustrate, Figure 1, Figure 2, and Figure 3 show our derived 2020 building height data at 10-m resolution.

2.3 Prior Physical Vulnerability

The physical vulnerability of Quezon City's building stock, characterised herein as building material typology, has been refined across two successive exposure developments. In the 2014 GMMA-RAP, Bautista et al. (2014) addressed the absence of building-level material typology data by leveraging coarse-grained 2000 census surveys on roof material types, such as galvanised iron, tile, concrete, wood, and makeshift, and wall material types, such as concrete, wood, and makeshift. Bautista et al. (2014) expressed the composition of each building material typology as proportions of building counts and floor area per roof-wall combination within defined polygonal areas, as shown in Figure 5. The 2022 CDRA update adopted this representational detail while substantially enhancing its spatial precision through the integration of the latest

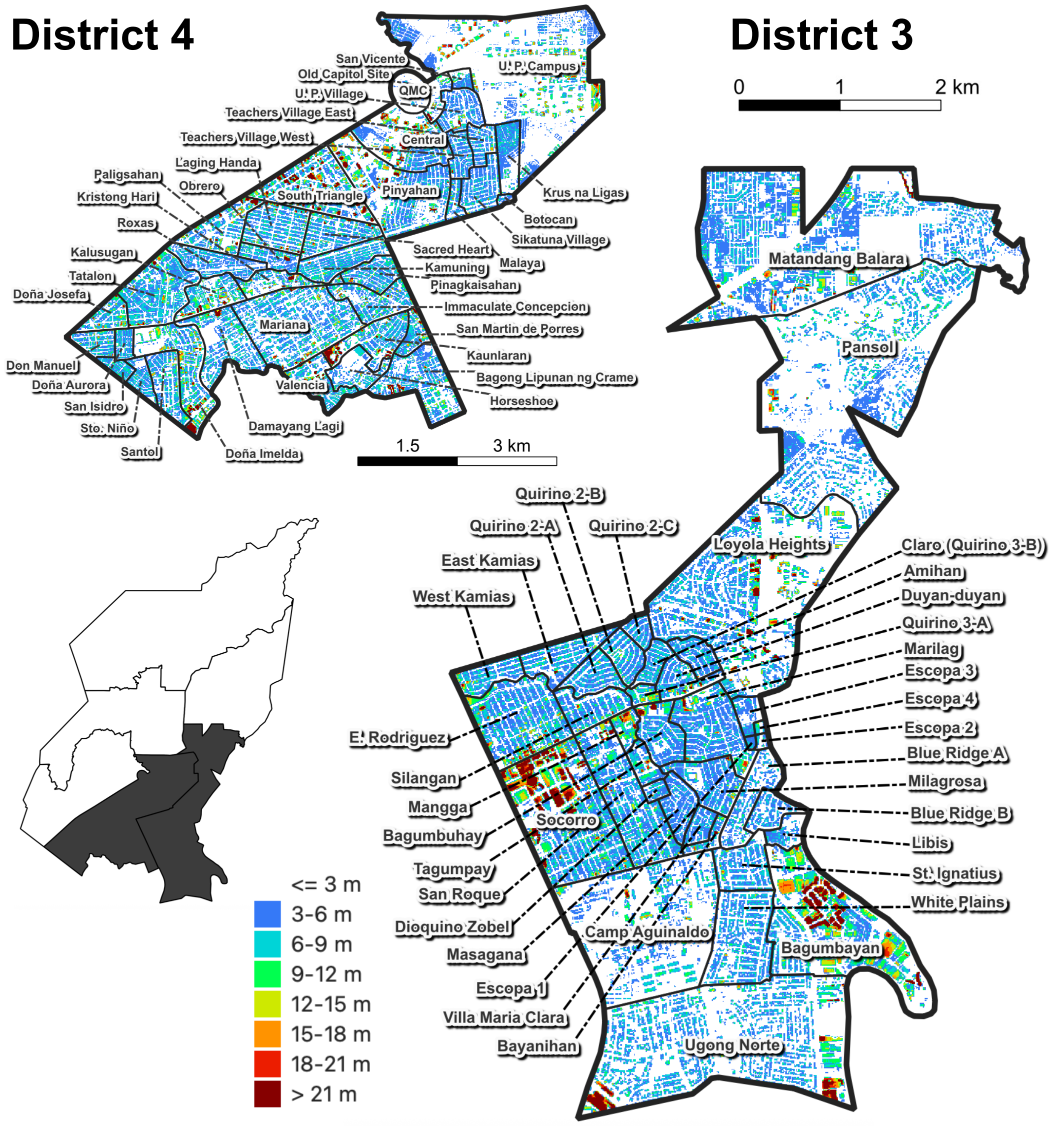

Figure 3: The administrative boundaries of barangays in Districts 3 and 4 (EMI 2022) showing our derived 2020 building height data at 10-m resolution.

digital elevation and surface models and high-resolution orthoimagery (EMI 2022). While each roof-wall combination corresponds to a physical vulnerability typology label, such as **C1L** for low-rise reinforced concrete moment frames, that can be synchronised with fragility and vulnerability functions in standard risk assessment (Bautista et al. 2012; Tingatinga et al. 2019),

Figure 4: Evolving exposure patterns of building height from the Google Open Buildings 2.5D Temporal dataset (Sirko et al. 2023) where the periods 2016-2021 and 2022-2030 serve as observations and projections, respectively.

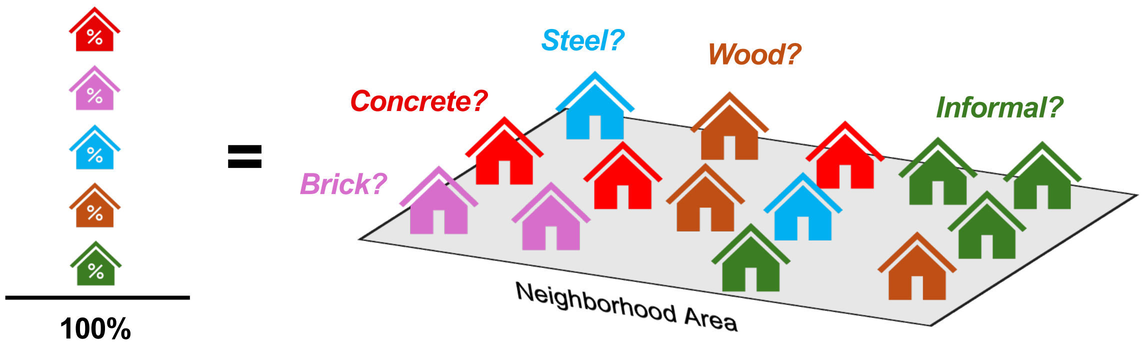

Figure 5: Schematic illustration of area-based approach.

the difficulty of one-to-one and one-to-many associations between roof-wall combinations and building material typologies remains a methodological challenge in ascertaining the true distribution of physical vulnerability. In other work, we addressed this difficulty using the combination of fuzzy mapping and deep learning-based spatial disaggregation using census as constraints to a clustering task (Dimasaka et al. 2026a), which is beyond the scope of this study. Nonetheless, this area-based approach can serve as a prior distribution for our probabilistic categorical assumption, enabling deep learning-based Bayesian updating toward a finer-grained spatiotemporal distribution of physical vulnerability across Quezon City.

Following the formulation from the preceding section, we rasterised the building material typology from the 2022 exposure database at a 10-m grid resolution, expressing the physical vulnerability (**V**) of each cell as a categorical random variable under a multinomial probability distribution as:

$$\mathbf{V} \sim \mathrm{Mult}(\boldsymbol{p}^1, \ldots, \boldsymbol{p}^K) \tag{2}$$

where $\boldsymbol{p}^1, \ldots, \boldsymbol{p}^K$ are the compositional values of $\mathbf{K}$ building typologies summing to 1.0 within each 10-m grid. Unlike the multi-temporal building exposure, the prior for physical vulnerability is static and non-time-varying across the 2016 to 2021 period, reflecting an underexplored opportunity in large-scale monitoring of building typologies using Earth observation data. In the same way, our graph-based deep neural network with parameters $\boldsymbol{\theta}$ transforms the prior parameters $(\boldsymbol{p}^1, \ldots, \boldsymbol{p}^K)$ into posterior estimates $(\boldsymbol{p}^1_\theta, \ldots, \boldsymbol{p}^K_\theta)$, enabling temporal inference for the period from 2016 to 2030. Recognising this current limitation brought about by the lack of temporal building typology data, this also presents an opportunity for future iteration for recalibration studies, when data becomes available.

We grouped these detailed typologies into broader material classification, as shown Table 1, and summarise their presence in each district and barangay in Table A.1, Table A.2, Table A.3, and Table A.4.

2.4 Multi-Hazard Scenarios

The compound effects of sequential hazards, wherein a large earthquake is followed by flooding or vice versa, are important in the multi-hazard context of Quezon City, where existing human settlements reside within and around an earthquake fault line, alongside recurring hydrometeorological hazards. Scenarios such as a major earthquake during the typhoon season or an impending typhoon landfall during the aftermath of a large earthquake could dramatically exacerbate risks to affected communities. To explore this compound risk scenario, we considered a magnitude-7.2 earthquake along the West Valley Fault in combination with a flooding simulation under the RCP8.5 with rainfall at a 100-year return period (EMI 2022). As shown in

Table 1: Building material classifications of detailed typologies.

Material	Symbol	Description
Wood	**W1W3**	Wooden light-frame (small)
	W2	Wooden light-frame (large)
	N	Makeshift or informal
Masonry	**CHBMWS**	Concrete hollow block
	URA	Unreinforced adobe walls
	URM	Unreinforced masonry walls
	RM2	Reinforced masonry walls with diaphragms
Concrete	**CWS**	Concrete with steel
	C1	Reinforced concrete moment frame
	C2	Reinforced concrete shear wall
	C4	Concrete shear walls and frames
	PC2	Precast concrete frames with shear walls
Steel	**S1**	Steel moment frames
	S2	Steel braced frames
	S3	Steel light frames

Figure 6, we adopted the hazard maps from the 2022 CDRA of EMI (2022) to have a consistent comparison across risk metrics.

2.4.1 M-7.2 West Valley Fault Earthquake Intensity Map

Described as the "Big One" in public discourse, the magnitude-7.2 earthquake scenario in the West Valley Fault is reportedly to have a return period between 400 and 600 years with an uncertainty range of 100-400 years, based on the paleoseismic studies by Nelson et al. (2000). Depending on the distance from the fault rupture and soil characteristics through which the earthquake propagates, Figure 6 (*left*) maps the Modified Mercalli Intensity (MMI) (Wood and Neumann 1931) (see Table 2 for descriptions) based on its empirical relationship with peak ground acceleration calculated from ground motion prediction models (EMI 2022).

2.4.2 RCP8.5 100-year Flood Depth Map

As established in the Quezon City Master Drainage Plan (EMI 2022), we used the flood depth map under the scenario of Representative Concentration Pathway (RCP) 8.5 (2020-2039) with rainfall at a 100-year return period, as shown in Figure 6 (*right*). The RCP8.5 scenario represents an upper-bound, business-as-usual trajectory characterised by the highest projected greenhouse gas concentrations, compounded by the absence of climate mitigation measures and sustained high population growth (Riahi et al. 2011). This is also comparable in intensity to the observed inundation from severe tropical storm Ondoy, known internationally as Ketsana (EMI 2022). The flood depth map is stratified into five increasing inundation levels: ($< 0.2m$) remain generally manageable; ($0.2 - 0.5m$) destabilise moving vehicles; ($0.5 - 1.5m$) pose casualty risks and disrupt light to medium vehicles; ($1.5 - 3.0m$) render households significantly non-functional; and ($> 3.0m$) displace residents to upper floor levels.

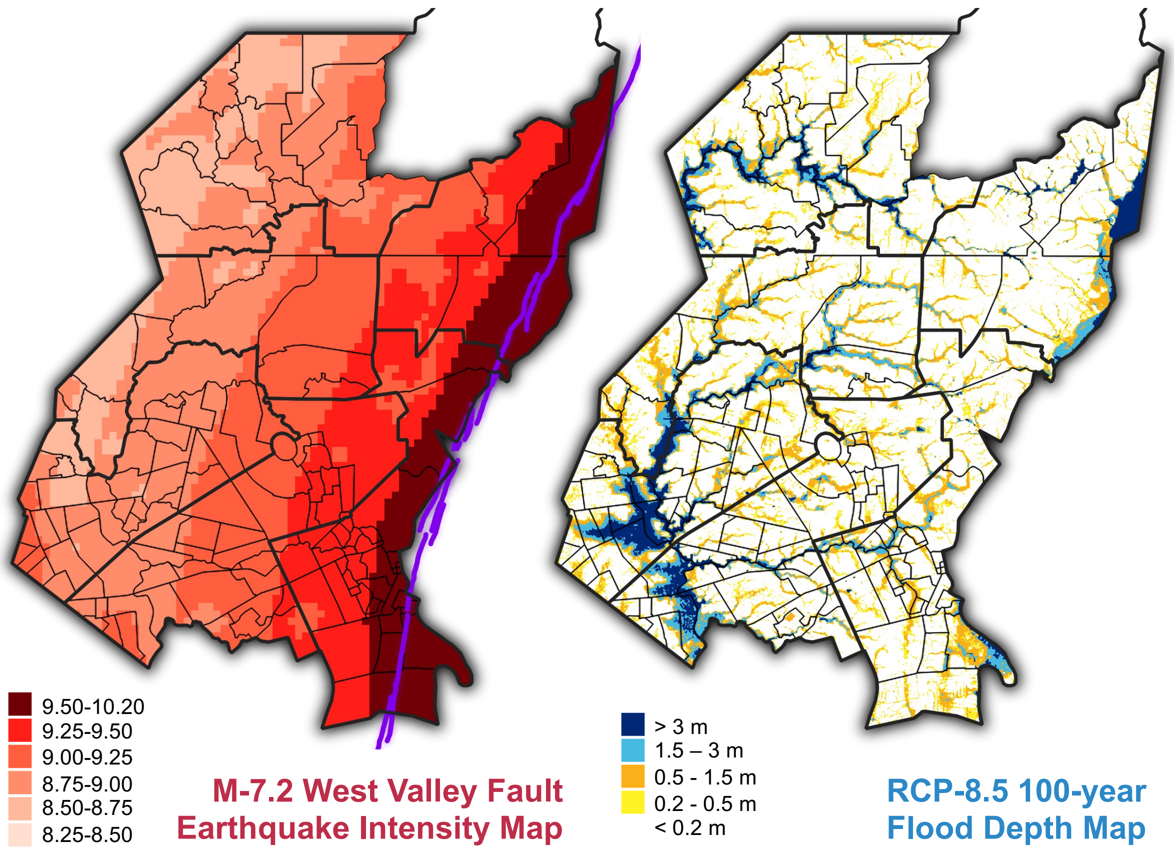

Figure 6: Multi-hazard scenarios (EMI 2022).

Table 2: Modified Mercalli Intensity Scale (Wood and Neumann 1931).

MMI	Description
8	"Damage **slight** in specially designed structures; **considerable** in ordinary substantial buildings with partial collapse; **great** in poorly built structures. Panel walls thrown out of frame structures. Fall of chimneys, factory stacks, columns, monuments, and walls. Heavy furniture overturned. Sand and mud ejected in small amounts. Changes in well water. Disturbed persons driving motor cars."
9	"Damage **considerable** in specially designed structures; well-designed frame structures thrown out of plumb; **great** in substantial buildings, with partial collapse. Buildings shifted off foundations. Ground cracked conspicuously. Underground pipes broken."
10	"Some well-built wooden structures **destroyed**; most masonry and frame structures **destroyed** with foundations; ground badly cracked. Rails bent. Landslides **considerable** from riverbanks and steep slopes. Shifted sand and mud. Water splashed (slopped) over banks."

3 Methods

3.1 Probabilistic Data-Driven Model of Exposure and Vulnerability

The probabilistic data-driven model, known as the Graph Variational State-Space Model provided in detail in Dimasaka et al. (2026b), trains four modules of graph-based deep neural

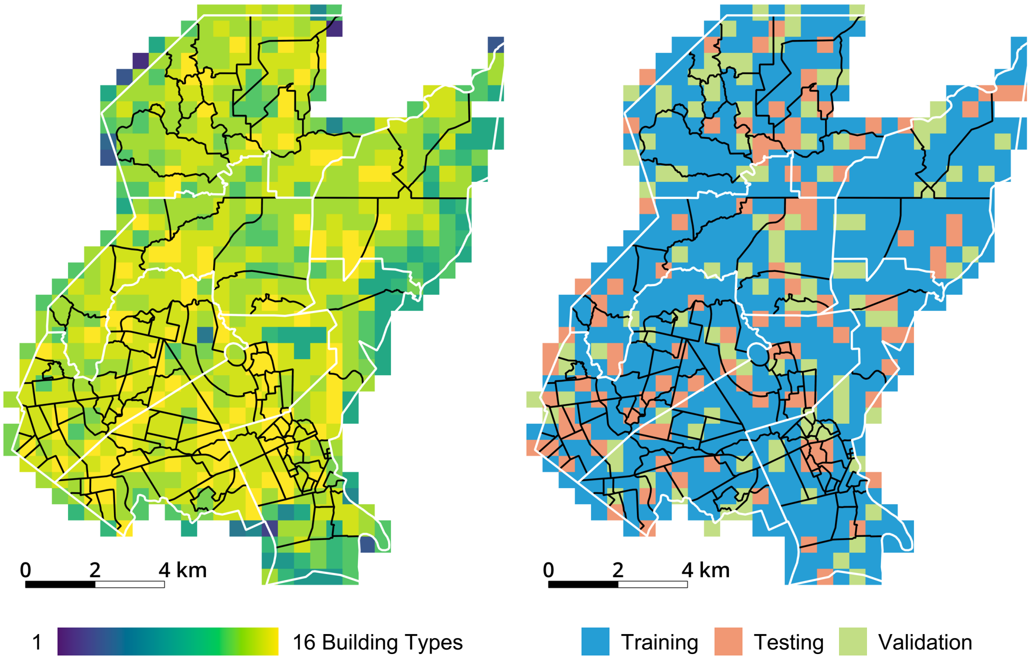

Figure 7: The varying number of building types (*left*) controls the splitting of dataset into training (70%), testing (15%), and validation (15%) sets (*right*).

network that approximates: (1) the relationship among the patterns of building height (exposure), input prior of material typology compositions (physical vulnerability), and other covariates from Copernicus Sentinel-2 imagery; and (2) the dynamics of posterior estimates for the lognormal and multinomial probability distributions of building exposure and physical vulnerability, respectively. Similar to Bayesian updating enhanced by probabilistic graph deep learning, it trains a set of parameters $\boldsymbol{\theta}$ for each posterior distribution by balancing new information across temporal periods against the prior information from the Google Open Buildings 2.5D Temporal dataset and the Quezon City's building stock with material typology characterisation.

The graph-structured representation of building exposure and physical vulnerability incorporates neighbourhood information from eight-directional adjacency[1] among 10-m pixels, establishing a learning propagation mechanism as the parameters $\boldsymbol{\theta}$ of a three-layer graph convolutional neural network[2] (Kipf and Welling 2016) converge to an optimal solution. In each module of physical vulnerability, the variational autoencoder[3] learns a structured[4] latent[5] representation consistent with the discrete categorical (i.e., multinomial) nature of physical vulnerability, extending the analytical Bayesian formulations of Pittore et al. (2020) and Porter et al. (2014) through the reparameterisation trick of Jang et al. (2016). Model training optimises the combined loss[6] comprising the reconstruction of decoded patterns, a Kullback-Leibler divergence loss[7] for the encoded posterior distributions of building exposure and physical vulnerability, and a semi-supervised cross-entropy loss (Kingma et al. 2014). As the number of available building material typologies varies across barangays (see Table A.1, Table A.2, Table A.3, Table A.4), we considered non-overlapping tiles of size 48x48 grid cells, split into training (70%), testing (15%), and validation (15%) sets, as shown in Figure 7.

[1] eight directions: north, east, west, south, northeast, southeast, southwest, and northwest
[2] a type of graph-based deep neural network
[3] a deep learning solution that approximates the posterior estimates
[4] "structured" means the use of parameters of a probability distribution
[5] similar to the term"hidden" because the true compositions are not fully observed (or available)
[6] "loss" measures similarity against available observations
[7] a metric that compares the parameters of two probability distributions (i.e., prior vs posterior)

Table 3: Inverse-step weighting approach.

		Inference														
		2016	2017	2018	2019	2020	2021	2022	2023	2024	2025	2026	2027	2028	2029	2030
Observations	2016	1	1/2	1/3	1/4	1/5	1/6	1/7	1/8	1/9	1/10	1/11	1/12	1/13	1/14	1/15
	2017		1	1/2	1/3	1/4	1/5	1/6	1/7	1/8	1/9	1/10	1/11	1/12	1/13	1/14
	2018			1	1/2	1/3	1/4	1/5	1/6	1/7	1/8	1/9	1/10	1/11	1/12	1/13
	2019				1	1/2	1/3	1/4	1/5	1/6	1/7	1/8	1/9	1/10	1/11	1/12
	2020					1	1/2	1/3	1/4	1/5	1/6	1/7	1/8	1/9	1/10	1/11
	2021						1	1/2	1/3	1/4	1/5	1/6	1/7	1/8	1/9	1/10

For downstream inference, the trained model was applied to newly prepared overlapping tiles and aggregated pixel-wise to generate the final maps, producing six sets of probabilistic projections corresponding to each observed period from 2016 to 2021, each extending individually up to 2030. For example, the model conditioned on the 2016 observed measurement generates probabilistic projections for every period from 2017 to 2030, and similarly for each subsequent observed year. Because this produces multiple overlapping projections for any given future period, we applied a temporal weighting approach via $1/step$, wherein projections at closer temporal distance carry greater weight than those further from their conditioning observation, reflecting their comparatively higher reliability. To illustrate, a projection for 2017 conditioned on 2016 is just one step away and therefore weighted most heavily, while a projection for 2025 conditioned on 2016 is nine steps away and contributes proportionally less to the aggregated estimate. As shown in Table 3, this inverse-step weighting approach, when normalised column-wise, attempts to address the inherent imperfections of temporal prediction under limited historical observations, yielding a reliability-weighted composite map across the entire 2016-2030 horizon.

3.2 Earthquake and Flood Risk Assessment

Applying the same approach (Tingatinga et al. 2019; Allen et al. 2014) from the 2022 CDRA of EMI (2022) on the inferred annual posterior samples of building height (exposure) and material typology compositions (physical vulnerability) from 2016 to 2030, we calculated the distribution of earthquake-damaged floor area at varying states: **None**, **Slight**, **Moderate**, **Extensive**, and **Complete**, which is further classified into **Complete without Collapse** and **Complete with Collapse**.

The earthquake risk assessment follows the standard probabilistic approach (Baker et al. 2021; Cornell et al. 1968; FEMA 2022) wherein each damage state assumes a lognormal probability distribution that is parameterised through median and standard deviation of ground shaking intensity. In symbols,

$$P(\text{damage state} \mid \text{intensity}) = \Phi\left[\frac{1}{\text{standard deviation}} \ln\left(\frac{\text{intensity}}{\text{median}}\right)\right] \tag{3}$$

where Φ is the standard normal cumulative distribution function. Figure 6 (*left*) provides the input intensity. The parameters, median and standard deviation, for each damage state by material typology for the local building stock are available from Tingatinga et al. (2019) and FEMA (2022). To illustrate, Figure 8 plots the probability of *exceeding* the **Slight** damage state for a wooden light-frame building and describes the physical interpretation of each damage state in Table 4.

We calculated the probabilities of *exceedance* for all damage states, and evaluated their differences to obtain the probability of *being* in each damage state. For each grid cell, we

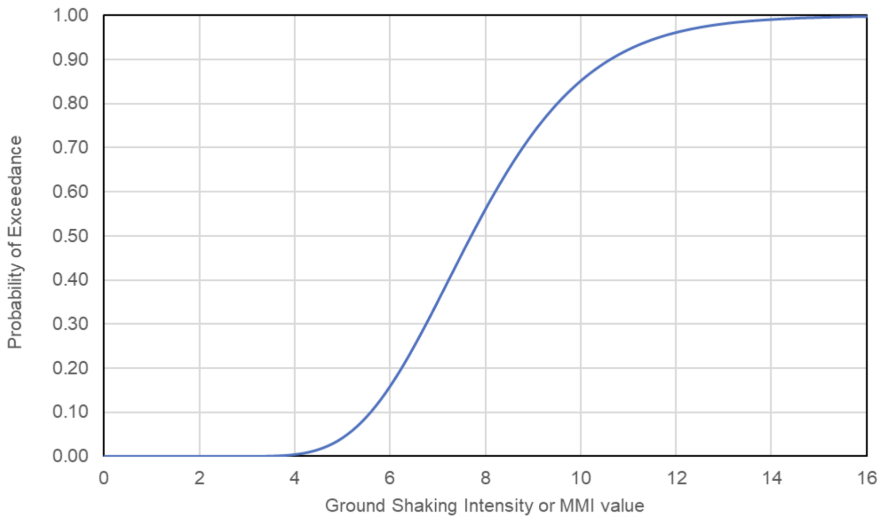

Figure 8: Example curve of lognormal distribution for the **Slight** damage state for a wooden light-frame building (adopted from (Dimasaka 2022).

Table 4: Physical interpretation of damage states for a wooden light-frame building FEMA (2022).

Damage State	Description
Slight	"Small plaster or gypsum-board cracks at corners of door and window openings and wall-ceiling intersections; small cracks in masonry chimneys and masonry veneer."
Moderate	"Large plaster or gypsum-board cracks at corners of door and window openings; small diagonal cracks across shear wall panels exhibited by small cracks in stucco and gypsum wall panels; large cracks in brick chimneys; toppling of tall masonry chimneys."
Extensive	"Large diagonal cracks across shear wall panels or large cracks at plywood joints; permanent lateral movement of floors and roof; toppling of most brick chimneys; cracks in foundations; splitting of wood sill plates and/or slippage of structure over foundations; partial collapse of "room-over-garage" or other "soft-story" configurations; small foundation cracks."
Complete	"Structure may have large permanent lateral displacement, may collapse, or be in imminent danger of collapse due to cripple wall failure or the failure of the lateral load-resisting system; some structures may slip and fall off the foundations; large foundation cracks."

multiply this probability of *being* in a particular damage state with the total floor area from our inferred posterior maps to estimate the corresponding damaged floor area.

Using the population rate per unit of floor area that is extrapolated and uniformly applied from various public statistics data (PSA 2026), we evaluated the corresponding casualties or injuries at increasing four severity levels, as shown in Table 5. In addition, we estimated the earthquake-induced displacement by using the population under the **Extensive** and **Complete** damage states. Similarly, the flood risk assessment deals with overlaying the map of buildings

Table 5: Injury classification scale (FEMA 2022).

Severity	Description
Slight Injuries	"Injuries requiring basic medical aid that could be administered by paraprofessionals. These types of injuries would require bandages or observation. Some examples are a sprain, a severe cut requiring stitches, a minor burn (first-degree or second-degree on a small part of the body), or a bump on the head without loss of consciousness."
Serious Injuries	"Injuries requiring a greater degree of medical care and use of medical technology such as x-rays or surgery, but not expected to progress to a life-threatening status. Some examples are third-degree burns or second-degree burns over large parts of the body, a bump on the head that causes loss of consciousness, or fractured bone."
Life-threatening Injuries	"Injuries that pose an immediate life-threatening condition if not treated adequately and expeditiously. Some examples are uncontrolled bleeding, punctured organ, other internal injuries, spinal column injuries, or crush syndrome."
Fatalities	"Instantaneously killed or mortally injured."

with one-to-two floor levels with the critical flood depth at 0.5 m, a threshold that triggers flood-induced displacement.

3.3 Derivation of Annual Development Profile Maps

We derived maps of annual development profiles that rank and classify barangays based on their 2016-2030 growth in built-up area, population, building material, earthquake risk, and multi-hazard human displacement. Using quintiles or five equal parts with around 28 barangays each, we described the growth tiers: **Lowest**, **Lower-Mid**, **Median**, **Upper-Mid**, and **Highest**. The annual development profile is expressed in two ways: (1) average annual increase in absolute measures and (2) compounded annual growth rate (CAGR) in percentage using:

$$\mathrm{CAGR} = \left(\frac{Y_\mathrm{T}}{Y_0}\right)^{\frac{1}{t_\mathrm{T}-t_0}} - 1 \tag{4}$$

where Y_0 and Y_T are measurements at time t_0 and t_T, respectively.

4 Results and Discussion

4.1 Annual Development Profiles

4.1.1 Annual Development Profile of Population and Building Exposure

Figure 9 shows local upward urbanization patterns by classifying 142 barangays in six districts into five tiers of annual growth in population and built-up floor area. Among all districts, **District 2** recorded the highest annual growth in built-up area at +2.12% (+180,308 m^2), followed by **District 5** at +1.81% (+234,479 m^2), although **District 5** has the larger annual increase in population at +1.07% (+6,254) than that of **District 2**. The results also show that, despite the lower growths, the remaining **District 1**, **District 3**, **District 4**, and **District 6** exhibit a more spatially sparse trend in built-up area, alongside localised growth in population, particularly noticeable in **District 1** at +1.21% (+5,219). This shows that the intra-city neighbourhood-level development has two distinct parts, wherein the northern portion exhibits a more balanced

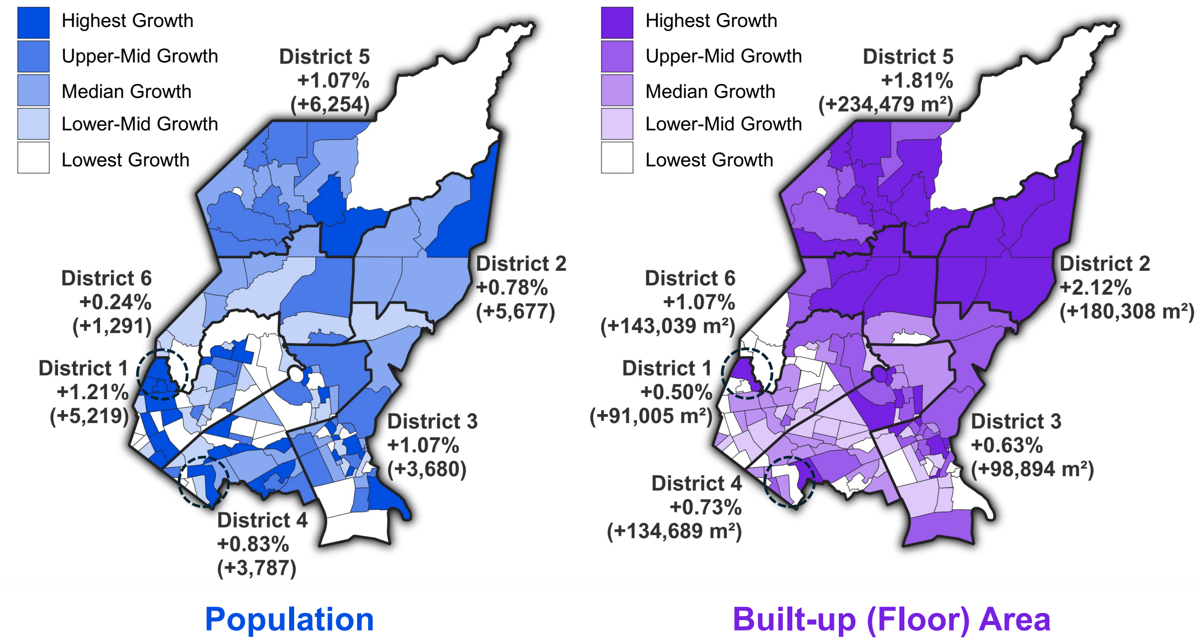

Figure 9: Annual development profile of population count (*left*) and building exposure (in terms of total built-up floor area) (*right*). The percentages are CAGR, and the numbers inside the parentheses are the average annual increase at the district level. The encircled areas are **Brgy. Balingasa** in **District 1** and **Brgy. Doña Imelda** in **District 4**.

upward growth for both increasing built-up area for growing population, and the southern portion implies a localised densification constrained by the slower growth in built-up area. Our findings further confirm the behavioural pattern of population growth with preferences to more developed areas, mostly located in the southern portion, which connects to other neighbouring urbanised cities in the Greater Metro Manila Area.

Examining further this observed localised densification in **District 1**, only one barangay, **Brgy. Balingasa**, belongs to the **Highest Growth** tier of built-up area, while 12 and 11 barangays are part of the **Lowest Growth** and **Median Growth** tiers. Despite that, in the same district, the population trends in 11 barangays are classified as **Highest Growth**, including **Brgy. Balingasa** in the **Upper-Mid Growth** tier. Another concerning case is **Brgy. Doña Imelda** in **District 4**, which recorded **Lowest Growth** in built-up area at +0.10% (+931 m^2) but overwhelmed by the **Highest Growth** in population at +5% (+1,067), notwithstanding the reported impacts in its riverine informal settlements after typhoon Ondoy in 2009 (Nunag 2009; Saloma-Akpedonu and Lao 2011). By understanding these trends in neighbourhood-level growth in built-up areas and population, our insights into the annual development profile enable comparative analysis at the barangay level with varying growth tiers and provide evidence for prospective local management policies on the degree of urban exposure, particularly when contextualized with past disasters.

4.1.2 Annual Development Profile of Building Material of Physical Vulnerability

Figure 10 presents the changing utilization of and projected demand for four dominant construction materials, namely, **Wood**, **Masonry**, **Concrete**, and **Steel**. Parallel to our previous findings in the built-up area, the northern portion, consisting of **District 2**, **District 5**, and the eastern half of **District 6** shows that the majority of their barangays exhibit **Upper-Mid Growth** and **Highest Growth**, across all material types. In contrast, a more spatially sparse distribution of such high tiers is observed in the southern portion, consisting of **District 1**, **District 3**, and **District 4**. Given that **Concrete** and **Steel** are relatively more expensive yet physically stronger

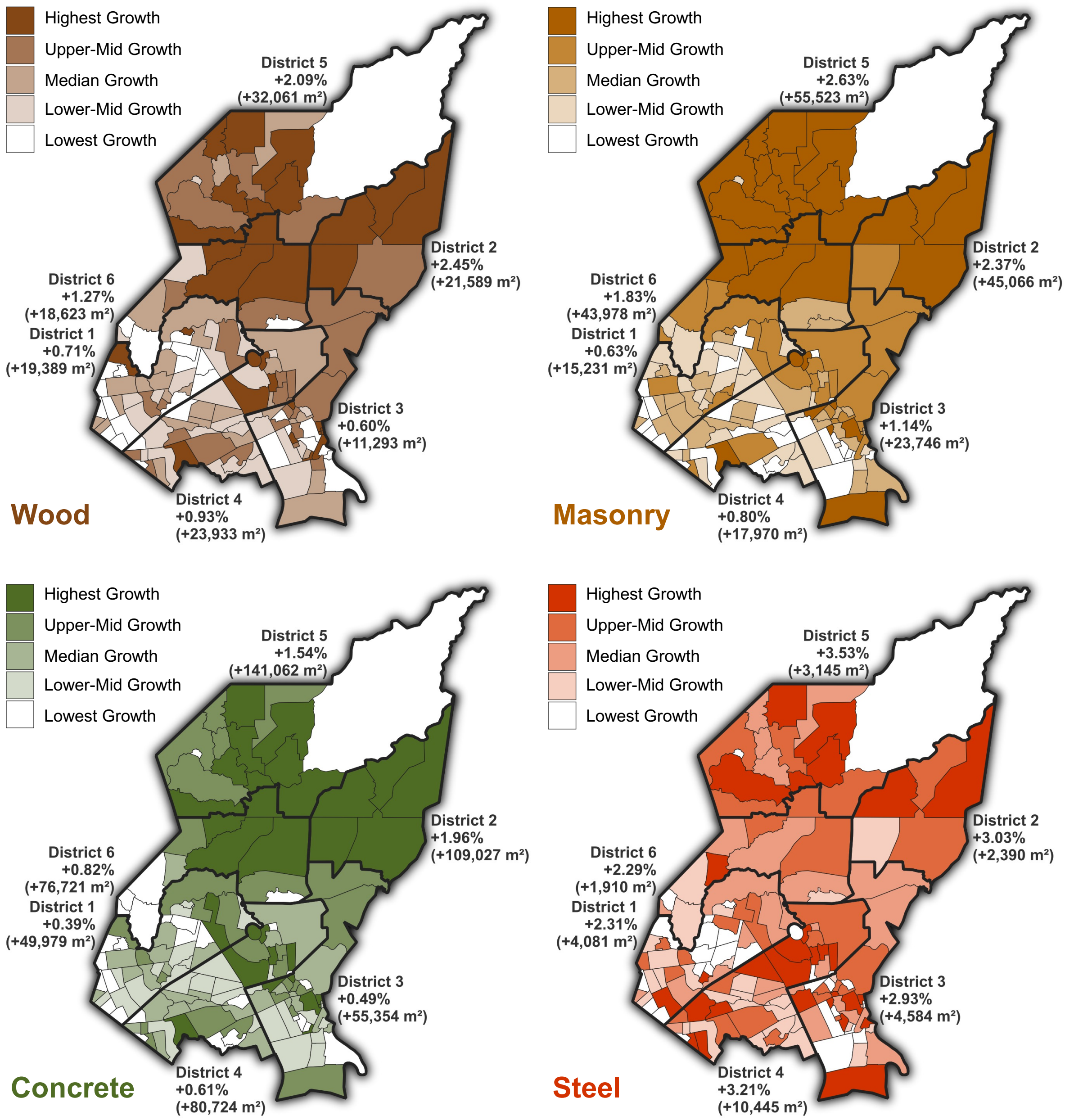

Figure 10: Annual development profile of physical vulnerability (in terms of dominant building material, see Table 1 for reference). The percentages are CAGR, and the numbers inside the parentheses are the average annual increase at the district level.

than **Wood** and **Masonry**, these growth patterns are also indicative of the urban distribution of affordability to certain types of building materials. Thus, rather than relying on a single city-wide regulation, this disaggregated evidence provides a basis for developing affordability-based interventions that incentivize the localized reduction of physical vulnerability, while reinforcing the role of local governments in ensuring compliance with building codes.

4.1.3 Annual Development Profile of Earthquake Risk by Building Damage States

While the preceding section provides evidence for the current limited feasibility in eliminating physically vulnerable buildings in practice, Figure 11 shows how local governments can simultaneously approach this with the evolving need for earthquake retrofits and recovery assistance programs by mapping the dynamics of expected damaged floor area, particularly

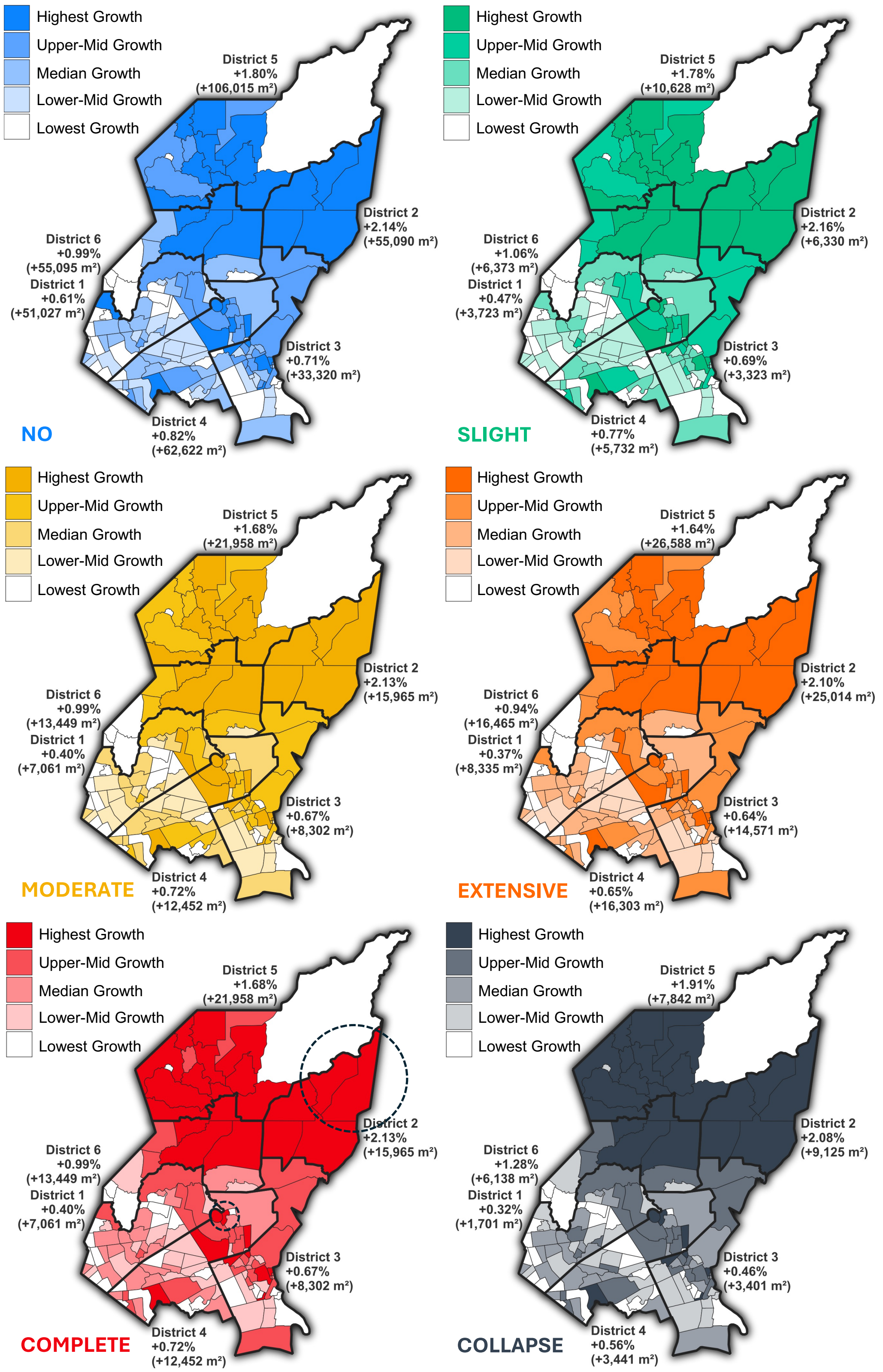

Figure 11: Annual development profile of earthquake risk (in terms of damaged floor area) by building damage state. In the bottom left, the encircled areas are the adjacent **Brgy. Payatas** and **Brgy. Bagong Silangan** in **District 2** and **Brgy. Old Capitol Site** in **District 4**.

under **Extensive**, **Complete**, and **Collapse** conditions. Across the city, **District 2** and **District 5** emerge to be dominated by barangays with **Highest Growth** under the **Complete** and **Collapse** damage states, and then **District 5** starts to increase its intra-district variability in growth tiers of their respective barangays under the less severe damage states of **Extensive**, **Moderate**, **Slight**, and **No**. To illustrate further, as the **Complete** damaged floor area in **District 2** annually increases by +2.13% (+15,965 m^2) (i.e., the highest among all districts), its top constituent barangays, **Brgy. Payatas** and **Brgy. Bagong Silangan**, also reported both about +3% (+10,815 m^2 and +15,595 m^2), respectively. These particular barangays, despite the reported largest increase in built-up floor area in Figure 9 (*right*), are also in proximity to the West Valley Fault line (see Figure 6 (*left*)) with relatively lower exposure to significant flood inundation (see Figure 6 (*right*)). This raises an important concern on the intersection between the recurrence of hazard (i.e, with flooding being more frequent than the unpredictable nature of earthquakes) and rapid exposure development of built-up areas, in the context of building material affordability, as we have also previously established in the preceding section.

However, it is also important to underscore the limitations of our trained data-driven model in predicting and projecting fine-grained material composition profiles and their subsequent earthquake risk analysis. As an example, while our results indicate that **Brgy. Old Capitol Site** in **District 4** recorded that its annual increase in **Complete** damaged floor area is in **Highest Growth** tier at +4.46% (+1,110 m^2), our investigation reveals that the trained data-driven model has a bias favouring prior distribution whose accuracy is derived from the area-based approach where a uniform compositional profile is attributed to a larger polygonal area (i.e., barangay's extent). In this case, if the prior distribution was mostly homogeneous (e.g., the majority of the built-up area is of the same building material, say **N** (makeshift or informal)), the resulting material composition of any new large-scale construction developments with unseen typology can entail a risk of inaccurate attribution. This is a particularly salient case where limitations can be further compounded in areas of contested development in **Brgy. Old Capitol Site** (Dovey and Recio 2024), reflecting a transitional interface of heightened heterogeneity in building material types between the expansion of informal settlements and the reclaiming of formally developed institutional areas. This evidence not only reveals the prevailing challenges in mapping fine-grained building material typology from a methodological standpoint, but also propagates the inherent equal-sharing assumptions within a polygon vis-à-vis privacy concerns originally embedded in census data. Whether the accuracy and applicability of our spatiotemporal results on the dynamics of vulnerability and risk are most appropriate at the building level or at the coarser barangay level should not undermine but rather acknowledge the existing poor socio-economic realities and vulnerabilities of informal settlements in **Brgy.**

Table 6: City-wide damaged floor area (EMI 2022) and our projection, in terms of average annual increase with CAGRs in parentheses for 2016-2021, 2021-2030, and 2016-2030, respectively.

Damage State Level	EMI (2022)	2016-2030 Projection (Our Study)
No	32,901,891 m^2 (39%)	+363,170 m^2 (+1.37%, +0.84%, +1.05%)
Slight	3,362,562 m^2 (4%)	+36,109 m^2 (+1.38%, +0.81%, +1.03%)
Moderate	7,831,161 m^2 (9%)	+79,186 m^2 (+1.23%, +0.82%, +0.98%)
Extensive	11,404,898 m^2 (13%)	+107,275 m^2 (+1.10%, +0.82%, +0.92%)
Complete without Collapse	25,959,077 m^2 (31%)	+265,025 m^2 (+1.44%, +0.76%, +1.01%)
Complete with Collapse	3,250,628 m^2 (4%)	+31,649 m^2 (+1.41%, +0.72%, +0.99%)
Total	84,710,217 m^2 (100%)	+882,414 m^2 (+1.34%, +0.80%, +1.01%)

Table 7: Top ten barangays with the highest damaged floor area (m^2) in the **Complete with Collapse** damage state (EMI 2022) and our projection, in terms of average annual increase with CAGR for 2016-2030 and its corresponding growth tier from Figure 11.

Barangays	**District**	**EMI (2022)** ↓	**2016-2030 Projection (Our Study)**
Batasan Hills	2	193,220 m^2	+3,002 m^2 (+1.78%) - *Highest*
Pasong Tamo	6	121,196 m^2	+1,994 m^2 (+2.18%) - *Highest*
Ugong Norte	3	110,849 m^2	+477 m^2 (+0.54%) - *Median*
Bagong Silangan	2	105,578 m^2	+1,737 m^2 (+2.81%) - *Highest*
Tandang Sora	6	102,592 m^2	+1,704 m^2 (+1.92%) - *Highest*
Holy Spirit	2	97,605 m^2	+1,349 m^2 (+1.58%) - *Highest*
Commonwealth	2	93,535 m^2	+1,885 m^2 (+2.25%) - *Highest*
Bagumbayan	3	92,111 m^2	-315 m^2 (-0.29%) - *Lowest*
Payatas	2	92,038 m^2	+1,182 m^2 (+2.91%) - *Highest*
Matandang Balara	3	91,775 m^2	+872 m^2 (+1.13%) - *Upper-Mid*

Old Capitol Site. These barangays are encircled with dashed lines in Figure 11 to show their relative locations on the map.

Nonetheless, our work significantly extends the CDRA (EMI 2022) by enhancing the following key risk profiles in the city's Ecological Profile report (QCPDO 2022). In Table 6, we present three CAGRs to separate the 2016-2021 period with higher reliability than the 2021-2030 period because of the available multi-temporal exposure observation for the former period. Our results show close CAGR values across all damage states, which indicates that the current proportion and projected changes in damaged floor area are expected to remain with negligible absolute changes at the city level. The CAGRs for the 2021-2030 period tend to be conservatively smaller than the earlier 2016-2021 period because of the regional generalisation (or smoothing) of trends, captured by our trained data-driven model.

However, the CAGRs highly vary at the barangay level, particularly for the top ten barangays from the CDRA (EMI 2022). Considering the **Complete with Collapse** damage state, Table 7 not only confirms our previous insights about **Brgy. Bagong Silangan** and **Brgy. Payatas** in **District 2** that are both in **Highest Growth** tier, but also supplements the existing static risk analysis with growth projections and their relative ranks in relation to local prioritisation of PDRM planning. Another noteworthy case is the recorded negative CAGR for **Brgy, Bagumbayan**, which relates to a modelling limitation of our exposure projection. Upon closer investigation of the map, the heterogeneous urban patterns in **Brgy. Bagumbayan**, which houses the highly urbanised 'Eastwood City' with high-rise buildings alongside vulnerable informal settlements in proximity to the river and fault line, introduce non-trivial neighbourhood variability to the training and generalisation mechanism of the data-driven model. For example, the shadows of a high-rise building and the orientation of raw Copernicus Sentinel-2 imagery, from which the Google Open Buildings 2.5 Temporal dataset was derived (Sirko et al. 2023), can result in erroneous predictions of multi-temporal building height values. Hence, similar to **Brgy. Old Capitol Site**, such a complicated transitional interface with highly varying geometrical and optical characteristics has to be considered carefully for broader urban studies applying Earth observation data.

To conclude, unlike conventional average annualised loss (AAL) metrics from probabilistic catastrophe risk practice, which annualise the economic loss by considering the full volatility of large earthquake events from a hazard-centric standpoint, our results demonstrate that annualised risk metrics can also be derived from the evolving spatiotemporal patterns of exposure and vulnerability under a contextualised emergency preparedness scenario of a

Table 8: City-wide injuries and fatalities (EMI 2022) and our projection, in terms of average annual increase with CAGRs in parentheses for 2016-2021, 2021-2030, and 2016-2030, respectively. The percentages in the EMI 2022 column refer to the proportion with respect to the entire city population.

Severity Level	EMI (2022)	2016-2030 Projection (Our Study)
Slight Injuries	104,955 (3.24%)	+773 (+0.43%, +0.99%, +0.77%)
Serious Injuries	35,618 (1.10%)	+255 (+0.40%, +0.96%, +0.75%)
Life-threatening Injuries	6,317 (0.19%)	+43 (+0.37%, +0.93%, +0.71%)
Injuries for Hospitalisation[a]	41,935 (1.29%)	+298 (+0.40%, +0.96%, +0.74%)
Fatalities	12,494 (0.39%)	+85 (+0.36%, +0.93%, +0.71%)

[a] Injuries for Hospitalisation = Serious Injuries + Life-threatening Injuries

magnitude-7.2 earthquake. These uncertainties across hazard, exposure, and vulnerability collectively constitute the key inputs to a whole probabilistic regional risk analysis, enabling an opportunity for shared and cooperative risk transfer financing mechanisms, such as risk pools for barangays, cities, and countries, that extend beyond the traditional household-level practice. As evidenced by the high variability of growth tiers across the six damage states in Figure 11, this further supports the diversification of regional risk under scenario-based hazard, when aggregating barangays with varying economic capacities into local risk pools for financing and recovery programs, which reflects the inherently shared and transboundary nature of disaster risk. In this way, our work not only extends the conventional risk profile with temporal insights derived from Earth Observation data, but also serves as a large-scale baseline underscoring the value of calibrating observed trends against empirical evidence to ensure the reliability in practice.

4.1.4 Annual Development Profile of Earthquake Risk by Injury and Fatality

Shifting our focus from damaged floor areas, this section integrates barangay population trends with changes in built-up areas to estimate the expected annual increase in **Slight**, **Serious**, and **Life-threatening** injuries, including **Fatalities**, thereby informing the prospective design of healthcare centres and hospital beds for post-disaster first-aid response. Figure 12 shows that, among all districts, **District 1**, **District 3**, and **District 4** record a high number of barangays with **Highest Growth** across all severity levels, followed by **District 5** for most of its barangays in the **Upper-Mid Growth** tier. These are spatially consistent with the patterns of population growth in Figure 9 (*left*). Our results further support the pressing need for healthcare centres, which remains below the target ratio of 1:20,000 (QCPDO 2022), specifically that **District 1**, **District 3**, and **District 4**, and **District 5** have shortfalls of 1, 7, 10, and 18 healthcare centres, respectively.

In the same way, Table 8 and Table 9 also enhance the CDRA of EMI (2022) with projected annual increases and CAGRs for casualty metrics. Our results indicate that an additional +298 beds would be necessary every year for injuries requiring hospitalisation, which incrementally increases the EMI baseline estimate of 41,935. Table 8 also shows that **Life-threatening** injuries at 6,317 growing by +43 annually can be prioritised, but the number of **Serious** injuries at 35,618 growing by +255 annually can potentially overwhelm the capacity of healthcare centres. The smaller CAGRs in the 2016-2021 period relative to that of the 2021-2030 period are also consistent with the reported annual population growth at 0.17% (2015-2020) and 0.99% (2020-2024) from official census records (PSA 2025). Table 9 also extends the identified top 10 barangays with annual growth rates to support local prospective design of barangay healthcare capacity, revealing that casualties in the majority of these barangays are in the **Lower-Mid**

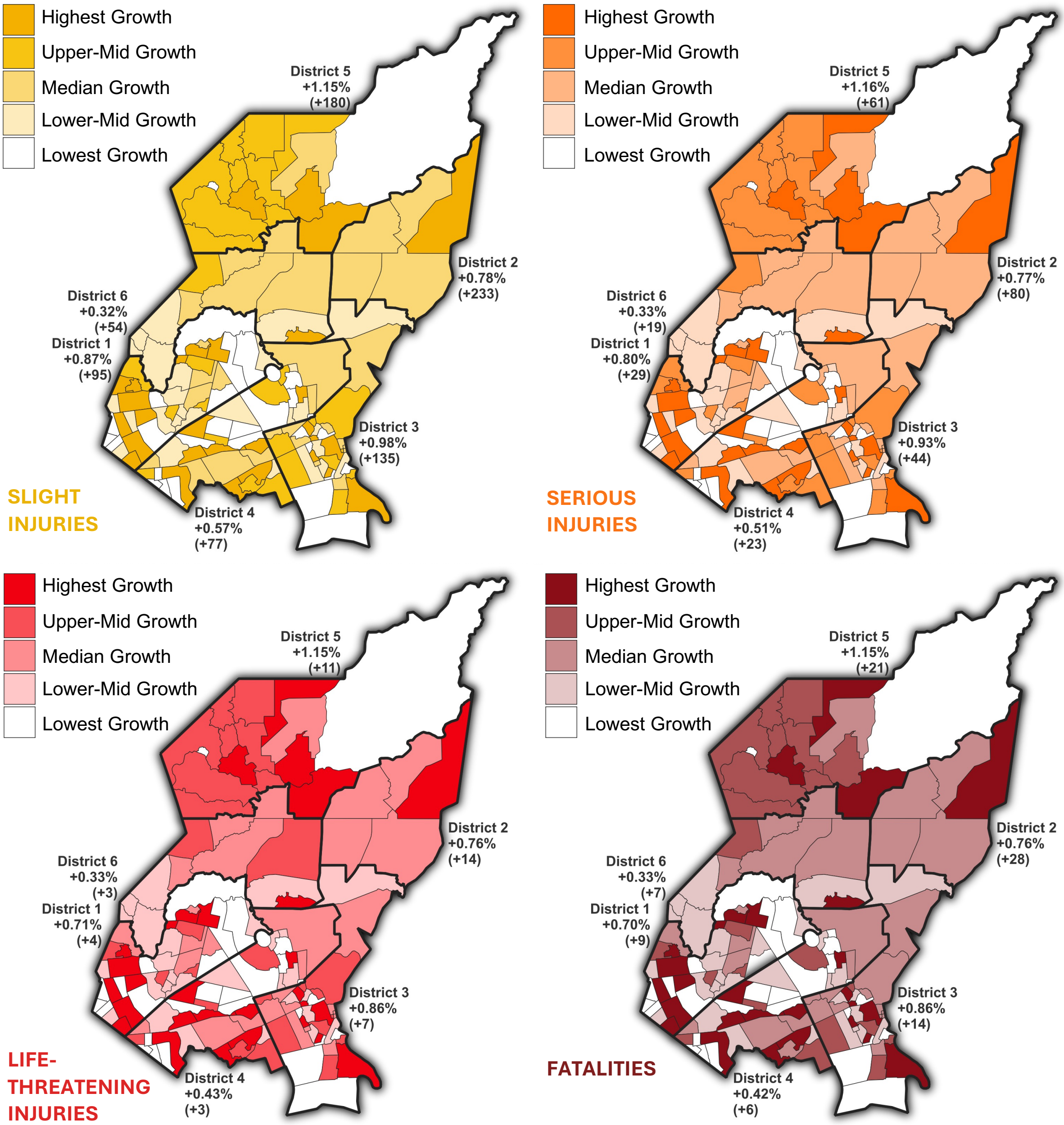

Figure 12: Annual development profile of earthquake risk in terms of casualties.

Growth and **Median Growth** tiers, except for **Brgy. Bagong Silangan**. The observed negative results for **Brgy. Culiat** and **Brgy. Matandang Balara** can be explained by the declining and slow growth of barangay population in the census years of 2015, 2020, and 2024 (PSA 2026). However, these results of contrasting tiers do not undermine the existing risk profiles of the top ten barangays, but rather indicate an intrinsic stability of their high population and casualty proportion. Beyond these results, despite the reported satisfactory city's current capacity at 8,845 beds against the standard benchmark of about 3,000 (i.e., 1 bed is to 1,000 residents) (QCPDO 2022), our analysis takes the scenario of M-7.2 earthquake, which implies a sudden demand and shock to the healthcare sector. This not only reinforces the one-time importance of emergency preparedness and investment in the city's healthcare sector in addressing such large casualties, but also underscores that the accessibility and adequacy of hospital beds in healthcare centres will remain an urgent and yearly responsibility.

Table 9: Top ten barangays with highest injuries and fatalities (EMI 2022) and our projection, in terms of average annual increase with CAGR for 2016-2030 and its corresponding growth tier from Figure 12.

Barangays	District	Serious Injuries	Life-threatening Injuries	Fatalities
Batasan Hills	2	3,085 (+13, +0.4%) *Median*	563 (+2, +0.5%) *Median*	1,116 (+5, +0.5%) *Median*
Commonwealth	2	2,485 (+14, +0.6%) *Median*	447 (+3, +0.6%) *Median*	885 (+5, +0.6%) *Median*
Payatas	2	1,874 (+11, +0.6%) *Median*	329 (+2, +0.6%) *Median*	649 (+4, +0.6%) *Median*
Pasong Tamo	6	1,741 (+12, +0.8%) *Median*	316 (+2, +0.8%) *Upper-Mid*	626 (+4, +0.8%) *Upper-Mid*
Bagong Silangan	2	1,714 (+37, +2.0%) *Highest*	307 (+6, +2.0%) *Highest*	607 (+13, +2.0%) *Highest*
Holy Spirit	2	1,521 (+5, +0.3%) *Median*	273 (+1, +0.3%) *Median*	541 (+2, +0.3%) *Median*
Tandang Sora	6	1,076 (+1, +0.1%) *Median*	194 (+0.2, +0.1%) *Median*	385 (+0.3, +0.1%) *Median*
Culiat	6	1,049 (-1, -0.2%) *Lower-Mid*	188 (-0.2, -0.1%) *Lower-Mid*	371 (-0.5, -0.1%) *Lower-Mid*
Matandang Balara	3	1,003 (-2, -0.2%) *Lower-Mid*	180 (-0.5, -0.3%) *Lower-Mid*	356 (-1, -0.3%) *Lower-Mid*
Bagbag	5	745 (+6, +1.3%) *Upper-Mid*	130 (+1, +1.3%) *Upper-Mid*	257 (+2, +1.2%) *Upper-Mid*

4.1.5 Annual Development Profile of Multi-Hazard Human Displacement

Human displacement under the compounding effects of a large earthquake and extreme flooding poses a significant risk to the social welfare, economic resources, and long-term development of a city (Eisner 2014). By classifying 142 barangays into terciles (i.e., three equal groups of increasing positive CAGRs), Figure 13 illustrates how varying annual growth rates in displacement reveal top barangays with large changes both from earthquake and flooding.

Our results show high correlation between earthquake- and flood-induced displacement growth rates, identifying the top 24 barangays (about 17% of 142) with the largest CAGRs, corresponding to 9, 5, 8, and 2 barangays in **District 1**, **District 3**, **District 4**, and **District 5**, respectively, as shown in Table 10. Figure 13 further differentiates some barangays with **HIGH** CAGR in earthquake- but **LOW** CAGR in flood-induced displacement, namely **Brgy. Lourdes** in **District 1** (+2.1%, +0.72%), and vice-versa, namely **Brgy. Krus na Ligas** in **District 4** (+0.40%, +2.7%). This evidence provides a prospective basis for the relative importance of dynamic risks from different hazards to which these barangays are exposed.

In the histograms showing the frequency distribution of barangay CAGRs in Figure 13, the noticeable negative CAGRs (i.e, to the left part and in white color) captured the fluctuations in local barangay population from the census years of 2015, 2020, and 2024 (PSA 2026). This indicates that the local population shows either a degree of demographic stability and unchanging patterns or a slight decline attributable to inter-neighbourhood movement. However, since the net population at the city level is growing (QCPDO 2022), our results, which identify 45 barangays (about 32% of 142) with non-positive CAGRs across earthquake- and flood-induced human displacement, would need further examination of their underlying population dynamics. In particular, the distinction between registered barangay inhabitants and the transient population, including residents commuting from neighbouring cities for employment opportunities, remains an underexplored aspect of displacement modelling at the local level.

Although EMI (2022) reported that the earthquake-induced displacement in **Brgy. Katipunan** ranks second-to-last in all 37 barangays in **District 1** with 1,031 displaced residents or about 37% of the local population, our findings reveal that its annual displacement growth from 2016 to 2030 is at +8.81% or increasing by +189 every year, due to its recent 2015-2020 densification reported in PSA (2026). This is further compounded by the flood-induced displacement growing at +11.4% (+216) every year. Upon closer inspection, our investigation shows that this large growth is attributed to the reported inconsistencies between the population census (PSA 2026) and official Records of Barangay Inhabitants (BRI) (QC 2025), which remains a contested discrepancy raised by the local government (QC 2021). Our study, which derives the local growth rate from the available temporal data from PSA (2026), underscores this challenge in casualty and displacement modelling at the local level in practice, in which

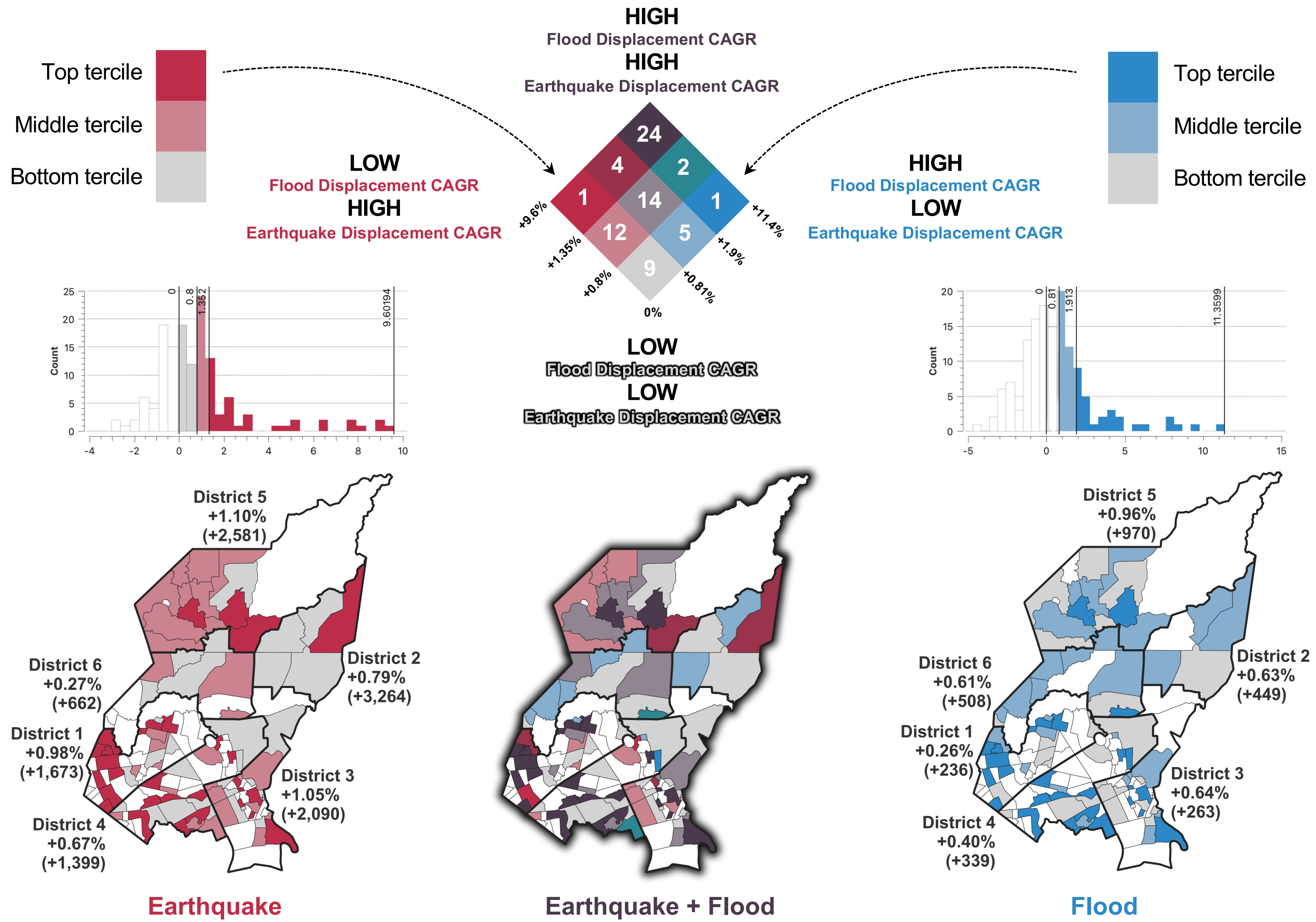

Figure 13: Annual development profile of multi-hazard human displacement under a magnitude-7.2 earthquake along the West Valley Fault in combination with a flooding simulation under the RCP8.5 with rainfall at 100-year return period.

Table 10: Top 24 barangays with **HIGH** earthquake- and **HIGH** flood-induced displacement growth in terms of average annual increase and CAGR.

		Annual Human Displacement Growth	
District	**Barangay**	**Earthquake**	**Flood**
1	Sta. Teresita	+613 (+9.6%)	+92 (+9.7%)
	Sto. Cristo	+709 (+8.9%)	+97 (+8.4%)
	Katipunan	+189 (+8.8%)	+216 (+11.4%)
	Kalusugan	+114 (+8.3%)	+41 (+7.9%)
	Marilag	+796 (+7.7%)	+50 (+5.7%)
	Damar	+75 (+7.7%)	+27 (+7.9%)
	Tagumpay	+117 (+6.6%)	+42 (+3.9%)
	Valencia	+420 (+6.5%)	+77 (+6.3%)
	Kaunlaran	+323 (+5.4%)	+6 (+2.9%)
3	Paligsahan	+147 (+5.2%)	+8 (+4.8%)
	Doña Imelda	+404 (+4.8%)	+326 (+4.3%)
	Bagumbayan	+599 (+4.4%)	+130 (+4.8%)
	Maharlika	+63 (+3.0%)	+52 (+2.2%)
	Sienna	+48 (+2.9%)	+38 (+2.3%)
4	Kristong Hari	+62 (+2.9%)	+34 (+3.6%)
	Manresa	+216 (+2.6%)	+111 (+2.4%)
	Pinagkaisahan	+65 (+2.4%)	+17 (+2.2%)
	Quirino 3-A	+17 (+2.3%)	+6 (+2.7%)
	Villa Maria Clara	+34 (+2.2%)	+20 (+2.0%)
	Teachers Village East	+42 (+2.0%)	+1 (+2.0%)
	Ramon Magsaysay	+110 (+1.8%)	+60 (+3.9%)
	North Fairview	+328 (+1.5%)	+120 (+2.1%)
5	Pag-ibig sa Nayon	+30 (+1.4%)	+3 (+3.7%)
	Gulod	+312 (+1.4%)	+366 (+2.1%)

the uncertainties in barangay population can propagate to a variety of downstream applications, such as risk-informed policymaking and social welfare prioritisation programs. Therefore, this evidence points to a broader and systemic data governance concern that extends not only in Quezon City but also to many local governments with limited technical capacities, thereby reinforcing that inter-agency validation must be in place to ensure a consistent and accurate representation of the local demography.

Notwithstanding these concerns on local population dynamics, our work provides additional temporal insights by extending the previously known city-wide displacement metrics (EMI 2022). Our results show that the earthquake-induced displacement of 1,561,765 or about 48% of the validated city population count of 3,242,298 is expected to annually grow by +11,670, a CAGR of +0.80%. Similarly, for population living in one-to-two floor levels, the current estimate of flood-induced displacement at 379,734 or about 12% of the city's population is expected to grow by +2,765, a CAGR of +0.59%. This evidence, derived from multi-temporal Earth Observation data, serves as a baseline for future work towards prospectively addressing the demand for temporary and permanent shelters under the compounding effects of earthquake and flooding.

4.2 Enhancing the Barangay Vulnerability Index with Dynamics

To support the local multi-hazard risk-informed decision-making of the city government, the EMI (2022) developed a composite index called Barangay Vulnerability Index (BVI) that identified hotspot barangays as a basis for local risk investment and prioritisation plans. In Table 11, we append our analysis to the top 14 barangays with the highest BVI under the compounding effects of earthquake and flooding. It is important to note that these results can serve as an initial large-scale analysis, which necessitates further careful validation to contextualise the significance of the reported average annual increase and CAGRs (in parentheses).

Nevertheless, a particular case, **Brgy. Bagumbayan**, which ranks top with the highest BVI, shows contradicting results wherein its annual earthquake damaged floor area growth falls in the **Lowest Growth** tier, in contrast to its casualty and displacement metrics in the **Highest Growth** tier. This is consistent with the previously observed heterogeneous urban patterns, which affect the modelling of building height. Despite that, **Brgy. Bagumbayan** and its 'Eastwood City' development have been extensively documented in many recent urban research as an 'exceptional' and 'exclusive' space (Karaan 2016; Kleibert and Kippers 2016; Kleibert 2018), wherein over-densifying high-income development concentrates population growth in proximity to both hazard zones while deploying narratives of 'sustainability' and 'inclusive development' that exclude the low-income communities most exposed to earthquake and flood risk. **Brgy. Bagumbayan** intersects the West Valley Fault line on the western side, while substantially exposed to river flooding on the eastern side. This explains the sudden increase in population as well as the corresponding annual growth in earthquake casualties and multi-hazard displacement in Table 11. More recently, Ancheta et al. (2025) reported an increase in zonal values around the area, which further marginalises the urban poor in **Brgy. Bagumbayan** and surrounding neighbourhoods, resulting in an increased number of informal settlements in the margins of such 'exclusive' developments (Ortega 2014). With this important context behind these quantified growth rates, our work provides a multi-hazard risk-informed evidence wherein such urban developments concentrate population exposure toward hazard zones. Our findings show that, by analysing urban patterns and their multi-hazard risk dynamics, it is imperative that equitable local development planning address the amplification of risk as a direct consequence of "exceptional" and "exclusive" spatial development.

4.3 Upgrading the Geospatial Exposure Database

Using the multi-temporal building height data both from the Google Open Buildings 2.5D Temporal dataset (Sirko et al. 2023) and our projection modelling, our work offers a potential large-scale upgrade of the existing geospatial exposure database of EMI (2022). Figure 14 illustrates the spatial distribution of under- and over-estimated building height values across five barangays, validated against Google Street View imagery. The floor levels of mid- to high-rise buildings in **Brgy. Katipunan**, **Brgy. Kaunlaran**, and **Brgy. Balingasa** were found to be underestimated, alongside a uniform one-floor assignment to adjacent houses in **Brgy. Escopa 4** where two-floor structures are prevalent. Conversely, sparse overestimation of floor levels was identified in makeshift and informal settlements in **Brgy. Payatas**. Recognising that the CDRA is equally reliable at the time of its implementation for its use of the latest digital elevation and surface models and high-resolution orthoimagery, our work instead identifies strategic hotpots where upgrading can be prioritized for an improved characterisation of building attributes for more accurate risk assessments.

Table 11: Annual growth rates of earthquake-damaged floor area, casualties, and multi-hazard displacement across barangay vulnerability tiers, ranked by Barangay Vulnerability Index (BVI) (EMI 2022). The numbers outside and inside the parentheses are average annual increase and CAGRs, respectively, with corresponding tiers italicised. Note that careful validation must be in place to contextualise the significance of these growth metrics derived from Earth Observation.

					Annual Earthquake Damaged Floor Area Growth			Annual Earthquake Casualty Growth			Annual Multi-Hazard Displacement Growth	
Tier	Rank	Barangay	BVI	Dist.	Extensive	Complete	Collapse	Serious Injuries	Life-threatening Injuries	Fatalities	Earthquake	Flood
Tier 1 Very High Vulnerability	1	Bagumbayan	100	3	−911 (−0.3%) *Lowest*	−4,147 (−0.3%) *Lowest*	−315 (−0.3%) *Lowest*	+12 (+4.4%) *Highest*	+2 (+4.5%) *Highest*	+4 (+4.5%) *Highest*	+599 (+4.4%) *Top*	+130 (+4.8%) *Top*
	2	Claro (Quirino 3-B)	98	3	+140 (+0.9%) *Upper-Mid*	+278 (+0.8%) *Median*	+31 (+0.8%) *Upper-Mid*	−0.2 (−0.5%) *Lower-Mid*	−0.05 (−0.5%) *Lower-Mid*	−0.1 (−0.5%) *Lower-Mid*	−9 (−0.4%) *Non-positive*	−7 (−0.3%) *Non-positive*
	3	St. Peter	97	1	+131 (+0.4%) *Median*	+493 (+0.6%) *Median*	+45 (+0.5%) *Median*	−0.3 (−0.6%) *Lower-Mid*	−0.05 (−0.6%) *Lower-Mid*	−0.1 (−0.6%) *Lower-Mid*	−11 (−0.6%) *Non-positive*	−34 (−1.6%) *Non-positive*
	4	Quirino 2-B	93	3	+200 (+1.1%) *Upper-Mid*	+685 (+1.2%) *Upper-Mid*	+85 (+1.2%) *Upper-Mid*	+1 (+1.7%) *Highest*	+0.2 (+1.7%) *Highest*	+0.4 (+1.7%) *Highest*	+42 (+1.7%) *Top*	+24 (+1.8%) *Middle*
	5	Libis	92	3	+26 (+0.3%) *Lower-Mid*	+25 (+0.1%) *Lowest*	+7 (+0.2%) *Lower-Mid*	+1 (+1.1%) *Upper-Mid*	+0.2 (+1.1%) *Upper-Mid*	+0.3 (+1.1%) *Upper-Mid*	+31 (+1.0%) *Middle*	+18 (+1.2%) *Middle*
Tier 2 High Vulnerability	6	Masagana	86	3	−43 (−0.3%) *Lowest*	−116 (−0.2%) *Lowest*	−16 (−0.2%) *Lowest*	−0.1 (−0.1%) *Lower-Mid*	−0.02 (−0.1%) *Lower-Mid*	−0.03 (−0.1%) *Lower-Mid*	−3 (−0.1%) *Non-positive*	−8 (−0.5%) *Non-positive*
	7	Quirino 2-C	81	3	+138 (+1.8%) *Highest*	+487 (+1.9%) *Highest*	+59 (+1.8%) *Highest*	+1 (+1.3%) *Upper-Mid*	+0.1 (+1.3%) *Upper-Mid*	+0.2 (+1.3%) *Upper-Mid*	+23 (+1.3%) *Middle*	+10 (+0.8%) *Middle*
	8	East Kamias	81	3	+534 (+1.5%) *Highest*	+1,222 (+1.5%) *Highest*	+135 (+1.4%) *Highest*	+0.2 (+0.2%) *Median*	+0.03 (+0.2%) *Median*	+0.05 (+0.2%) *Median*	+10 (+0.3%) *Bottom*	−5 (−0.3%) *Non-positive*
	9	Villa Maria Clara	80	3	+3 (+0.04%) *Lowest*	+16 (+0.1%) *Lowest*	−0.1 (0.00%) *Lowest*	+1 (+2.2%) *Highest*	+0.2 (+2.1%) *Highest*	+0.3 (+2.1%) *Highest*	+34 (+2.2%) *Top*	+20 (+2.0%) *Top*
Tier 3 Moderate Vulnerability	10	Silangan	80	3	+237 (+0.9%) *Upper-Mid*	+619 (+0.8%) *Upper-Mid*	+60 (+0.7%) *Upper-Mid*	+0.1 (+0.2%) *Median*	+0.02 (+0.2%) *Median*	+0.03 (+0.1%) *Median*	+8 (+0.3%) *Bottom*	+1 (+0.1%) *Bottom*
	11	Quirino 3-A	61	3	+54 (+0.5%) *Median*	+181 (+0.6%) *Median*	+18 (+0.5%) *Median*	+0.4 (+2.3%) *Highest*	+0.1 (+2.2%) *Highest*	+0.1 (+2.2%) *Highest*	+17 (+2.3%) *Top*	+6 (+2.7%) *Top*
	12	Bagumbuhay	60	3	+246 (+0.7%) *Median*	+936 (+0.9%) *Upper-Mid*	+94 (+0.8%) *Upper-Mid*	−0.05 (−0.1%) *Lower-Mid*	−0.01 (−0.1%) *Lower-Mid*	−0.03 (−0.1%) *Lower-Mid*	−1 (−0.03%) *Non-positive*	−10 (−0.7%) *Non-positive*
	13	Mangga	57	3	+221 (+0.9%) *Upper-Mid*	+188 (+0.3%) *Lower-Mid*	−3 (−0.05%) *Lowest*	−0.3 (−2.0%) *Lowest*	−0.05 (−2.2%) *Lowest*	−0.1 (−2.2%) *Lowest*	−9 (−1.6%) *Non-positive*	−5 (−4.7%) *Non-positive*
	14	Quirino 2-A	55	3	+138 (+0.5%) *Median*	+163 (+0.5%) *Median*	+21 (+0.5%) *Median*	−0.2 (−0.6%) *Lower-Mid*	−0.04 (−0.6%) *Lower-Mid*	−0.1 (−0.6%) *Lower-Mid*	−14 (−0.6%) *Non-positive*	−10 (−0.7%) *Non-positive*

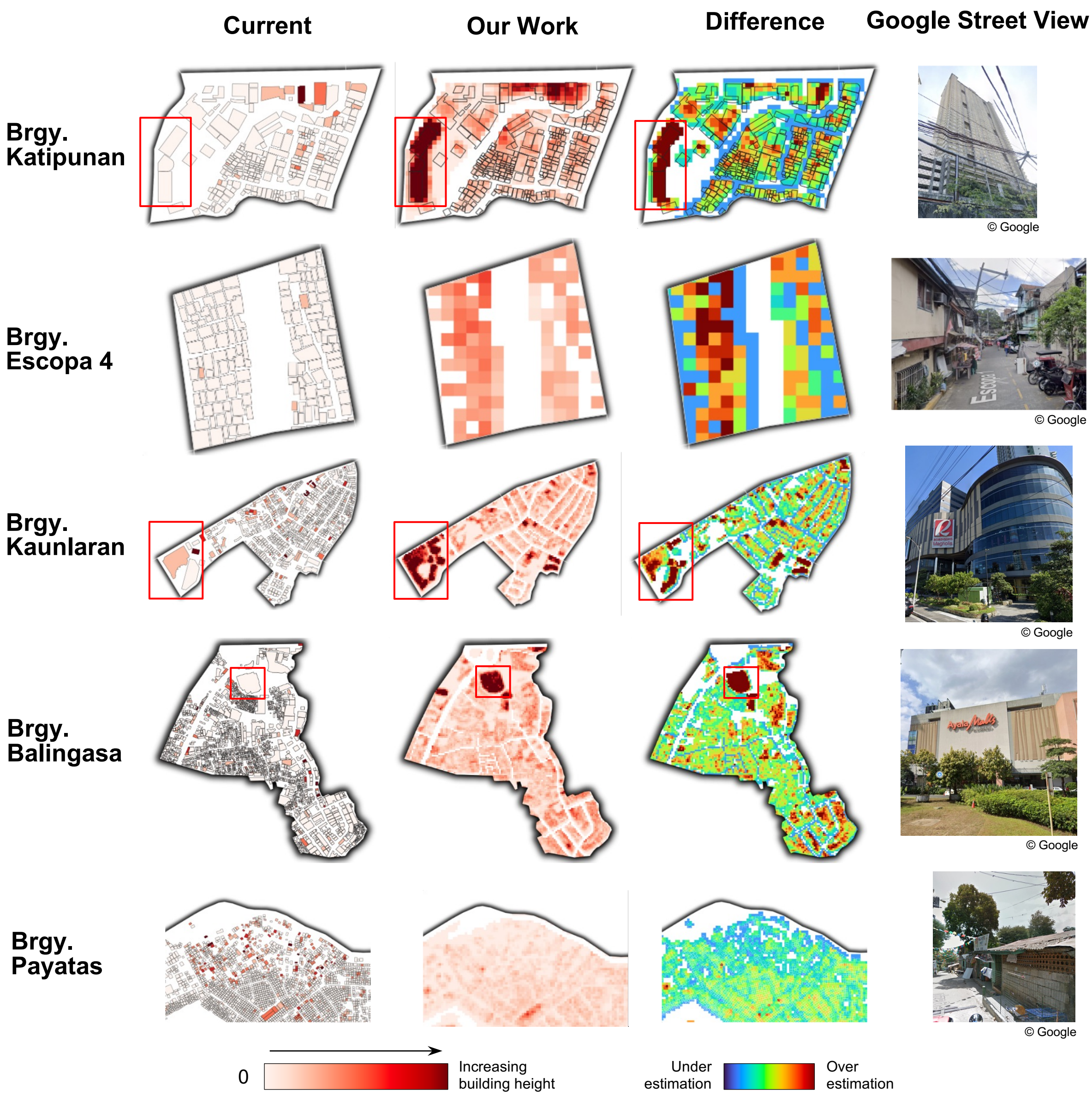

Figure 14: Five example barangays with observed noticeable difference in building heights (in increasing red colour) between the CDRA (EMI 2022) and our work. The colours in difference maps indicate underestimation (blue), overestimation (red), and negligible (green).

5 Conclusion and Future Work

This work examined the reliability of a geospatial database of building exposure and physical vulnerability, with particular attention to their spatiotemporal dynamics for climate and disaster risk assessment (CDRA), an increasingly central backbone of many prospective local government plans. Through a case study of Quezon City, Philippines, the primary aim was to demonstrate how the integration of multi-temporal Earth Observation data within a risk assessment framework advances the current state of practice in CDRA, towards a comprehensive understanding of multi-hazard urban risk dynamics across the neighbourhood-to-city scale. Key findings revealed that the derived annual development profiles underscored the value of disaggregated distributions of growth in building materials, damaged floor area, and casualty estimates in the implementation of affordability-based building code compliance, the design of retrofitting and recovery assistance programmes, and the assessment of healthcare sector capacity, amidst the rapidly growing urban population. The analysis further contributed to the understanding of the trajectory of city-wide and neighbourhood-level earthquake risk metrics across varying damage states, demonstrating the viability of prospective disaster risk management under evolving exposure and vulnerability patterns. The investigation into the risk dynamics and historical development in **Brgy. Bagumbayan** provided a multi-hazard risk-informed evidence in support of more equitable local development planning. The comparison against the existing geospatial exposure database opened an opportunity for the strategic improvement of building attribute characterisation. This research acknowledges limitations, such as the propagated uncertainties from the limited static prior distribution of physical vulnerability and multi-temporal exposure data, particularly in highly heterogeneous urban patterns. Additionally, the casualty and displacement modelling largely relied on the available multi-temporal national population data, which showed notable inconsistencies with official neighbourhood-level records. Future research directions should focus on the partial-to-complete incorporation of building-level attributes to refine the current static maps of physical vulnerability. Integrating additional temporal building datasets, localised population proxies, and satellite-derived embeddings would further enhance the building-level accuracy. In conclusion, the increasing adoption of digital mapping technologies for CDRA demands sustained scientific scrutiny and rigorous validation to support effective prospective disaster risk management at the local level. Understanding how urban risk evolves in a multi-hazard context is essential to shaping equitable long-term development plans that remain relevant to the increasing exposure of the growing vulnerable population.

6 Data and Code Availability

The spatiotemporal data are publicly available at https://doi.org/10.5281/zenodo.16655873 (Dimasaka et al. 2025). The code is also accessible at https://github.com/riskaudit/GraphVSSM under the MIT license.

Acknowledgments

This work is funded by the UKRI Centre for Doctoral Training in Application of Artificial Intelligence to the study of Environmental Risks (AI4ER) (EP/S022961/1). We are thankful for the building exposure and physical vulnerability data from Earthquakes and Megacities Initiative (through Urban Resilience Fellowship) (https://emi-megacities.org/) and Quezon City Disaster Risk Reduction and Management Office (through Ms. Maria Bianca Perez) (https://quezoncity.gov.ph/departments/quezon-city-disaster-and-risk-reduction-management-office/).

References

Allen T, Ryu H, Bautista B, et al (2014) Component 5 - Earthquake Risk Analysis. Enhancing Risk Analysis Capacities for Flood, Tropical Cyclone Severe Wind and Earthquake for the Greater Metro Manila Area. Philippine Institute of Volcanology and Seismology, Geoscience Australia

Amaratunga D, Sridarran P, Haigh R, et al (2019) The progress of local governments in making cities resilient: state of play. Global Assessment Report on Disaster Risk Reduction (GAR 2019), United Nations Office for Disaster Risk Reduction (UNDRR) pp 1–24

Ancheta JA, Magno-Ballesteros M, Ramos TP (2025) Urban revitalization and shelter inadequacy: A geospatial analysis. Tech. rep., PIDS Discussion Paper Series

Baker J, Bradley B, Stafford P (2021) Seismic hazard and risk analysis. Cambridge University Press

Basu M, Srivastava N, Mulyasari F, et al (2013) Making cities and local governments ready for disasters: A critical overview of a recent approaches. Risk, Hazards & Crisis in Public Policy 4(4):250–273

Bautista ML, Bautista B, Narag I, et al (2014) Component 2 - Exposure Information Development. Enhancing Risk Analysis Capacities for Flood, Tropical Cyclone Severe Wind and Earthquake for the Greater Metro Manila Area. Philippine Institute of Volcanology and Seismology, Geoscience Australia

Bautista MLP, Bautista BC, Narag IC, et al (2012) Strengthening natural hazard risk assessment capacity in the Philippines. Tech. rep., Geoscience Australia: Canberra

Cabi NS, Thomson T, Gascoigne J, et al (2021) How earth observation informs the activities of the re/insurance industry on managing flood risk. In: Earth Observation for Flood Applications. Elsevier, p 165–193

Chang SE, Yip JZ, Tse W (2019) Effects of urban development on future multi-hazard risk: The case of vancouver, canada. Natural Hazards 98(1):251–265

Cornell CA, et al (1968) Engineering seismic risk analysis. Bulletin of the Seismological Society of America 58(5):1583–1606

Costa DG, Bittencourt JCN, Oliveira F, et al (2024) Achieving sustainable smart cities through geospatial data-driven approaches. Sustainability 16(2):640

Cremen G, Galasso C, McCloskey J (2022) A simulation-based framework for earthquake risk-informed and people-centered decision making on future urban planning. Earth's Future 10(1):e2021EF002388

Cremen G, Galasso C, McCloskey J, et al (2023) A state-of-the-art decision-support environment for risk-sensitive and pro-poor urban planning and design in tomorrow's cities. International Journal of Disaster Risk Reduction 85:103400

Cremen G, Gentile R, Dabeek J, et al (2026) Multi-hazard disaster impact analysis outputs from synthetic future urban scenarios in 10 cities

Dimasaka J (2022) Towards an Equitable Development of the Regional Earthquake Resilience of the Greater Metro Manila Area, Philippines. Stanford Digital Repository, Public Policy Program, https://doi.org/doi/10.25740/kd110gb2567

Dimasaka J, Geiß C, So E (2025) A City-Scale Dataset of Annual Spatiotemporal Maps of Building Exposure and Physical Vulnerability in Quezon City, Philippines (2016–2030) via Graph Variational State-Space Model (GraphVSSM) . https://doi.org/10.5281/zenodo.16655873

Dimasaka J, Geiß C, So E (2026a) Deepc4: Deep conditional census-constrained clustering for large-scale multitask spatial disaggregation of urban morphology. arXiv:2507.22554

Dimasaka J, Geiß C, So E (2026b) Graphvssm: Graph variational state-space model for probabilistic spatiotemporal inference of dynamic exposure and vulnerability for regional disaster resilience assessment. Proceedings of the AAAI Conference on Artificial Intelligence

40(45):38376–38384

Dovey K, Recio R (2024) Informal Settlement on UP Diliman Campus. Tech. rep., UP-Center for Integrative and Development Studies

Eisner R (2014) Managing the risk of compound disasters. In: Disaster risk management in Asia and the Pacific. Routledge, p 157–187

EMI (2022) Climate and Disaster Risk Assessment Report for Quezon City: Climate Change, Earthquake, Flood, and Landslide Hazards, including Identification of Hotspot Barangays. Tech. rep., Quezon City Government and Earthquakes and Megacities Initiative

FEMA (2022) HAZUS Earthquake Model Technical Manual 5.1. Tech. rep., Federal Emergency Management Agency, United States

Freire S, Aubrecht C, Wegscheider S (2013) Advancing tsunami risk assessment by improving spatio-temporal population exposure and evacuation modeling. Natural hazards 68(3):1311–1324

Gignac-Eddy A, Gomes I, Ponte E, et al (2020) Guidance Note on Using the Probabilistic Country Risk Profiles for Disaster Risk Management. Tech. rep., CIMA Research Foundation and International Centre on Environmental Monitoring

Glazer T, Hacheme GQ, Zaytar A, et al (2025) TEMPO: Global Temporal Building Density and Height Estimation from Satellite Imagery. arXiv preprint arXiv:251112104

HLURB (2013) CLUP Guidebook: A Guide to Comprehensive Land Use Plan Preparation (Volume 1: The Planning Process). Tech. rep., Housing and Land Use Regulatory Board

HLURB (2015) Supplemental Guidelines on Mainstreaming Climate Change and Disaster Risks in the Comprehensive Land Use Plan). Tech. rep., Housing and Land Use Regulatory Board

Hou Z, Zhang J, Zhang M, et al (2023) Hospital-system functionality quantification based on supply–demand relationship under earthquake. Natural Hazards 116(1):213–234

Huyck CK, Hu Z, Eguchi M, et al (2022) Characterizing uncertainty of general building stock exposure data. Earthquake Spectra 38(3):2008–2025

Jang E, Gu S, Poole B (2016) Categorical reparameterization with gumbel-softmax. arXiv:161101144

Karaan AKI (2016) Negotiating Spaces of Exception: Metro Manila's Planned Unit Developments, the Case of Eastwood City. PhD thesis, University of Sheffield, Department of Urban Studies and Planning

Kingma DP, Mohamed S, Jimenez Rezende D, et al (2014) Semi-supervised learning with deep generative models. Adv Neural Inf Process Syst 27

Kipf TN, Welling M (2016) Semi-supervised classification with graph convolutional networks. arXiv:160902907

Kleibert JM (2018) Exclusive development (s): Special economic zones and enclave urbanism in the philippines. Critical Sociology 44(3):471–485

Kleibert JM, Kippers L (2016) Living the good life? the rise of urban mixed-use enclaves in metro manila. Urban Geography 37(3):373–395

Lagmay AMA, Santiago JT, Mendoza JE (2024) Mainstreaming climate and disaster risk assessment in the comprehensive land use plan. In: Climate Emergency in the Philippines: Impacts and Imperatives for Urgent Policy Action. Springer, p 311–336

Lee Y, Kim J (2026) Multi-hazard exposure prioritization with time-varying population: Integrating seismic amplification susceptibility and flood hazards in seoul. Applied Sciences

Loos S, Lallemant D, Baker J, et al (2020) G-dif: A geospatial data integration framework to rapidly estimate post-earthquake damage. Earthquake Spectra 36(4):1695–1718

Malalgoda C, Amaratunga D, Haigh R (2016) Overcoming challenges faced by local governments in creating a resilient built environment in cities. Disaster Prevention and Management: An International Journal 25(5):628–648

Marconcini M, Metz-Marconcini A, Esch T, et al (2021) Understanding current trends in global urbanisation-the world settlement footprint suite. GI_Forum 9(1):33–38

McGuire RK (2001) Deterministic vs. probabilistic earthquake hazards and risks. Soil Dynamics and Earthquake Engineering 21(5):377–384

Nelson AR, Personius SF, Rimando RE, et al (2000) Multiple large earthquakes in the past 1500 years on a fault in metropolitan manila, the philippines. Bulletin of the Seismological Society of America 90(1):73–85

Nunag A (2009) Riverine informal settlement: Barangay Doña Imelda, Quezon City. Social Dimensions of the Impact of Typhoon Ondoy on Urban Poor Communities: Site Reports. Tech. rep., Institute of Philippine Culture, School of Social Sciences, Loyola Schools, Ateneo de Manila University

Ortega AA (2014) Mapping Manila's Mega-Urban Region. Asian Population Studies 10(2):208–235

Pesaresi M, et al (2024) Advances on the global human settlement layer by joint assessment of earth observation and population survey data. International Journal of Digital Earth 17(1):2390454

Pham HM, Yamaguchi Y, Bui TQ (2011) A case study on the relation between city planning and urban growth using remote sensing and spatial metrics. Landscape and urban planning 100(3):223–230

Pittore M, Haas M, Silva V (2020) Variable resolution probabilistic modeling of residential exposure and vulnerability for risk applications. Earthq Spectra 36(1_suppl):321–344

Porter K, Hu Z, Huyck C, et al (2014) User guide: Field sampling strategies for estimating building inventories. GEM Foundation

PSA (2025) Highlights of the National Capital Region (NCR) Population 2024 Census of Population (2024 POPCEN). URL https://psa.gov.ph/statistics/population-and-housing/node/1684077885/

PSA (2026) The population of the barangays in Quezon City by census years. URL https://www.citypopulation.de/en/philippines/quezoncity/

QC (2021) QC asks PSA to correct its "impossible" 2020 census data. URL https://quezoncity.gov.ph/qc-asks-psa-to-correct-its-impossible-2020-census-data-some-qc-barangays-supposedly-lost-50-of-population/

QC (2025) Barangay Katipunan. URL https://quezoncity.gov.ph/brgy-directory/katipunan/

QCPDO (2022) 2022 Quezon City Ecological Profile. Tech. rep., Quezon City Planning and Development Office, Quezon City Government

Quigley M, Duffy B (2020) Effects of earthquakes on flood hazards: a case study from christchurch, new zealand. Geosciences 10(3):114

Rentschler J, Avner P, Marconcini M, et al (2023) Global evidence of rapid urban growth in flood zones since 1985. Nature 622(7981):87–92

Riahi K, Rao S, Krey V, et al (2011) Rcp 8.5—a scenario of comparatively high greenhouse gas emissions. Climatic change 109(1):33

Saloma-Akpedonu C, Lao MEJ (2011) The Social Impacts of Tropical Storm Ondoy and Typhoon Pepeng. The recovery of communities in Metro Manila and Luzon. Tech. rep., Institute of Philippine Culture, School of Social Sciences, Loyola Schools, Ateneo de Manila University

Schorlemmer D, Oostwegel L, Calliku D, et al (2026) Every building on earth–the global dynamic exposure model. Preprint

Sirko W, Kashubin S, Ritter M, et al (2021) Continental-scale building detection from high resolution satellite imagery. arXiv preprint arXiv:210712283

Sirko W, Brempong EA, Marcos JT, et al (2023) High-resolution building and road detection from sentinel-2. arXiv preprint:231011622

Stalhandske Z, de Ruiter MC, Chambers J, et al (2025) Global assessment of population exposure to multiple climate-related hazards from 2003 to 2021: a retrospective analysis. The Lancet Planetary Health 9(8)

Tingatinga E, Pacheco B, Hernandez Jr J, et al (2019) Development of seismic vulnerability curves of key building types in the philippines. In: New Zealand Society for Earthquake Engineering Annual Conference

UNDRR (2025a) Global Assessment Report on Disaster Risk Reduction 2025: Resilience Pays: Financing and Investing for our Future. Tech. rep., United Nations Office for Disaster Risk Reduction, Geneva

UNDRR (2025b) UNDRR Strategic Framework 2026-2030. Tech. rep., United Nations Office for Disaster Risk Reduction, Geneva

United Nations Office for Disaster Risk Reduction (UNDRR) (2017) The Sendai Framework Terminology on Disaster Risk Reduction. "Disaster risk management". Accessed 16 April 2026

Wang K, Wu X, Chen THK, et al (2026) Mapping precipitation-triggered landslide risks in global human settlements. Applied Geography 187:103886

Wood H, Neumann F (1931) Modified Mercalli Intensity Scale of 1931. Seismological Society of America Bulletin 21:277–283

Woods D, McKeen T, Cunningham A, et al (2025) Global gridded multi-temporal datasets to support human population distribution modelling. Gates Open Research 9:72

Xia Z, Jia N, Yuan B, et al (2026) Long-term remote sensing reveals the development of informal settlements and their impact on land surface temperature in african drylands: A case study of windhoek, namibia. Sustainable Cities and Society p 107119

A Building Material Typology in Districts and Barangays

Table A.1: Building material typology in District 1 (EMI 2022), where the row and column of **N** refer to the number of building typologies present per barangay and per typology (across the city), respectively.

Material	Symbol	Description	N	Alicia	Bagong Pag-asa	Bahay Toro	Balingasa	Bungad	Damar	Damayan	Del Monte	Katipunan	Lourdes	Maharlika	Manresa	Mariblo	Masambong	N. S. Amoranto (Gintong Silahis)	Nayong Kanluran	Paang Bundok	Pag-ibig sa Nayon	Paltok	Paraiso	Phil-Am	Project 6	Ramon Magsaysay	Salvacion	San Antonio	San Isidro Labrador	San Jose	Sienna	St. Peter	Sta. Cruz	Sta. Teresita	Sto. Cristo	Sto. Domingo (Matalahib)	Talayan	Vasra	Veterans Village	West Triangle
				District 1 (37 barangays)																																				
Material	**Symbol**	**Description**	**N**	13	15	15	15	15	13	14	14	14	14	14	14	13	13	13	14	14	14	15	14	14	14	15	14	15	14	14	13	14	15	15	15	13	13	15	15	15
Wood	**W1W3**	Wooden light-frame (small)	142	•	•	•	•	•	•	•	•	•	•	•	•	•	•	•	•	•	•	•	•	•	•	•	•	•	•	•	•	•	•	•	•	•	•	•	•	•
	W2	Wooden light-frame (large)	142	•	•	•	•	•	•	•	•	•	•	•	•	•	•	•	•	•	•	•	•	•	•	•	•	•	•	•	•	•	•	•	•	•	•	•	•	•
	N	Makeshift or informal	141	•	•	•	•	•	•	•	•	•	•	•	•	•	•	•	•	•	•	•	•	•	•	•	•	•	•	•	•	•	•	•	•	•	•	•	•	•
Masonry	**CHBMWS**	Concrete hollow block	142	•	•	•	•	•	•	•	•	•	•	•	•	•	•	•	•	•	•	•	•	•	•	•	•	•	•	•	•	•	•	•	•	•	•	•	•	•
	URA	Unreinforced adobe walls	138	•	•	•	•	•	•	•	•	•	•	•	•	•	•	•	•	•	•	•	•	•	•	•	•	•	•	•		•	•	•	•		•	•	•	•
	URM	Unreinforced masonry walls	140	•	•	•	•	•	•	•	•	•	•	•	•	•	•	•	•	•	•	•	•	•	•	•	•	•	•	•	•	•	•	•	•	•	•	•	•	•
	RM2	Reinforced masonry walls with diaphragms	80		•	•	•	•												•		•				•		•			•		•	•	•	•		•	•	•
Concrete	**CWS**	Concrete with steel	142	•	•	•	•	•	•	•	•	•	•	•	•	•	•	•	•	•	•	•	•	•	•	•	•	•	•	•	•	•	•	•	•	•	•	•	•	•
	C1	Reinforced concrete moment frame	142	•	•	•	•	•	•	•	•	•	•	•	•	•	•	•	•	•	•	•	•	•	•	•	•	•	•	•	•	•	•	•	•	•	•	•	•	•
	C2	Reinforced concrete shear wall	142	•	•	•	•	•	•	•	•	•	•	•	•	•	•	•	•	•	•	•	•	•	•	•	•	•	•	•	•	•	•	•	•	•	•	•	•	•
	C4	Concrete shear walls and frames	142	•	•	•	•	•	•	•	•	•	•	•	•	•	•	•	•	•	•	•	•	•	•	•	•	•	•	•	•	•	•	•	•	•	•	•	•	•
	PC2	Precast concrete frames with shear walls	142	•	•	•	•	•	•	•	•	•	•	•	•	•	•	•	•	•	•	•	•	•	•	•	•	•	•	•	•	•	•	•	•	•	•	•	•	•
Steel	**S1**	Steel moment frames	142	•	•	•	•	•	•	•	•	•	•	•	•	•	•	•	•	•	•	•	•	•	•	•	•	•	•	•	•	•	•	•	•	•	•	•	•	•
	S2	Steel braced frames	114		•	•	•	•		•	•	•	•	•	•			•	•	•	•	•	•	•	•	•	•	•	•	•	•	•	•	•	•	•	•	•	•	•
	S3	Steel light frames	125	•	•	•	•	•	•	•	•	•	•	•	•	•	•		•		•	•	•	•	•	•	•	•	•	•		•	•	•	•			•	•	•

Table A.2: Building material typology in Districts 2, 5, and 6 (EMI 2022), where the row and column of **N** refer to the number of building typologies present per barangay and per typology (across the city), respectively.

Material	Symbol	Description		Bagong Silangan	Batasan Hills	Commonwealth	Holy Spirit	Payatas	Bagbag	Capri	Fairview	Greater Lagro	Gulod	Kaligayahan	Nagkaisang Nayon	North Fairview	Novaliches Proper	Pasong Putik Proper	San Agustin	San Bartolome	Sta. Lucia	Sta. Monica	Apolonio Samson	Baesa	Balong-bato	Culiat	New Era	Pasong Tamo	Sangandaan	Sauyo	Talipapa	Tandang Sora	Unang Sigaw
				District 2 (5)					District 5 (14 barangays)														District 6 (11)										
Material	**Symbol**	**Description**	**N**	14	15	15	15	15	15	14	15	15	15	15	15	15	15	15	15	15	14	15	15	15	13	15	15	15	15	14	15	15	13
Wood	**W1W3**	Wooden light-frame (small)	142	•	•	•	•	•	•	•	•	•	•	•	•	•	•	•	•	•	•	•	•	•	•	•	•	•	•	•	•	•	•
	W2	Wooden light-frame (large)	142	•	•	•	•	•	•	•	•	•	•	•	•	•	•	•	•	•	•	•	•	•	•	•	•	•	•	•	•	•	•
	N	Makeshift or informal	141	•	•	•	•	•	•	•	•	•	•	•	•	•	•	•	•	•	•	•	•	•	•	•	•	•	•	•	•	•	•
Masonry	**CHBMWS**	Concrete hollow block	142	•	•	•	•	•	•	•	•	•	•	•	•	•	•	•	•	•	•	•	•	•	•	•	•	•	•	•	•	•	•
	URA	Unreinforced adobe walls	138	•	•	•	•	•	•	•	•	•	•	•	•	•	•	•	•	•	•	•	•	•	•	•	•	•	•	•	•	•	•
	URM	Unreinforced masonry walls	140	•	•	•	•	•	•	•	•	•	•	•	•	•	•	•	•	•	•	•	•	•	•	•	•	•	•	•	•	•	•
	RM2	Reinforced masonry walls with diaphragms	80	•	•	•	•	•	•		•	•	•	•	•	•	•	•	•	•	•	•	•	•		•	•	•	•		•	•	
Concrete	**CWS**	Concrete with steel	142	•	•	•	•	•	•	•	•	•	•	•	•	•	•	•	•	•	•	•	•	•	•	•	•	•	•	•	•	•	•
	C1	Reinforced concrete moment frame	142	•	•	•	•	•	•	•	•	•	•	•	•	•	•	•	•	•	•	•	•	•	•	•	•	•	•	•	•	•	•
	C2	Reinforced concrete shear wall	142	•	•	•	•	•	•	•	•	•	•	•	•	•	•	•	•	•	•	•	•	•	•	•	•	•	•	•	•	•	•
	C4	Concrete shear walls and frames	142	•	•	•	•	•	•	•	•	•	•	•	•	•	•	•	•	•	•	•	•	•	•	•	•	•	•	•	•	•	•
	PC2	Precast concrete frames with shear walls	142	•	•	•	•	•	•	•	•	•	•	•	•	•	•	•	•	•	•	•	•	•	•	•	•	•	•	•	•	•	•
Steel	**S1**	Steel moment frames	142	•	•	•	•	•	•	•	•	•	•	•	•	•	•	•	•	•	•	•	•	•	•	•	•	•	•	•	•	•	•
	S2	Steel braced frames	114		•	•	•	•	•	•	•	•	•	•	•	•	•	•	•	•		•	•	•		•	•	•	•	•	•	•	
	S3	Steel light frames	125	•	•	•	•	•	•	•	•	•	•	•	•	•	•	•	•	•	•	•	•	•	•	•	•	•	•	•	•	•	•

Table A.3: Building material typology in District 3 (EMI 2022), where the row and column of **N** refer to the number of building typologies present per barangay and per typology (across the city), respectively.

				Amihan	Bagumbayan	Bagumbuhay	Bayanihan	Blue Ridge A	Blue Ridge B	Camp Aguinaldo	Claro (Quirino 3-B)	Dioquino Zobel	Duyan-duyan	E. Rodriguez	East Kamias	Escopa 1	Escopa 2	Escopa 3	Escopa 4	Libis	Loyola Heights	Mangga	Marilag	Masagana	Matandang Balara	Milagrosa	Pansol	Quirino 2-A	Quirino 2-B	Quirino 2-C	Quirino 3-A	San Roque	Silangan	Socorro	St. Ignatius	Tagumpay	Ugong Norte	Villa Maria Clara	West Kamias	White Plains
				District 3 (37 barangays)																																				
Material	**Symbol**	**Description**	**N**	13	14	14	13	12	12	15	13	13	13	14	15	12	12	13	13	13	15	15	13	13	15	15	14	15	14	14	13	15	15	15	13	14	14	14	14	14
Wood	**W1W3**	Wooden light-frame (small)	142	•	•	•	•	•	•	•	•	•	•	•	•	•	•	•	•	•	•	•	•	•	•	•	•	•	•	•	•	•	•	•	•	•	•	•	•	•
	W2	Wooden light-frame (large)	142	•	•	•	•	•	•	•	•	•	•	•	•	•	•	•	•	•	•	•	•	•	•	•	•	•	•	•	•	•	•	•	•	•	•	•	•	•
	N	Makeshift or informal	141	•	•	•	•	•	•	•	•	•	•	•	•	•	•	•	•	•	•	•	•	•	•	•	•	•	•	•	•	•	•	•	•	•	•	•	•	•
Masonry	**CHBMWS**	Concrete hollow block	142	•	•	•	•	•	•	•	•	•	•	•	•	•	•	•	•	•	•	•	•	•	•	•	•	•	•	•	•	•	•	•	•	•	•	•	•	•
	URA	Unreinforced adobe walls	138	•	•	•	•	•	•	•	•	•	•	•	•	•	•	•	•	•	•	•	•	•	•	•	•	•	•	•		•	•	•	•	•	•	•	•	•
	URM	Unreinforced masonry walls	140	•	•	•	•		•	•	•	•	•	•	•	•	•	•	•	•	•	•	•	•	•	•	•	•	•	•	•	•	•	•	•	•	•	•	•	•
	RM2	Reinforced masonry walls with diaphragms	80							•					•						•	•			•	•		•	•	•	•	•	•	•			•	•		
Concrete	**CWS**	Concrete with steel	142	•	•	•	•	•	•	•	•	•	•	•	•	•	•	•	•	•	•	•	•	•	•	•	•	•	•	•	•	•	•	•	•	•	•	•	•	•
	C1	Reinforced concrete moment frame	142	•	•	•	•	•	•	•	•	•	•	•	•	•	•	•	•	•	•	•	•	•	•	•	•	•	•	•	•	•	•	•	•	•	•	•	•	•
	C2	Reinforced concrete shear wall	142	•	•	•	•	•	•	•	•	•	•	•	•	•	•	•	•	•	•	•	•	•	•	•	•	•	•	•	•	•	•	•	•	•	•	•	•	•
	C4	Concrete shear walls and frames	142	•	•	•	•	•	•	•	•	•	•	•	•	•	•	•	•	•	•	•	•	•	•	•	•	•	•	•	•	•	•	•	•	•	•	•	•	•
	PC2	Precast concrete frames with shear walls	142	•	•	•	•	•	•	•	•	•	•	•	•	•	•	•	•	•	•	•	•	•	•	•	•	•	•	•	•	•	•	•	•	•	•	•	•	•
Steel	**S1**	Steel moment frames	142	•	•	•	•	•	•	•	•	•	•	•	•	•	•	•	•	•	•	•	•	•	•	•	•	•	•	•	•	•	•	•	•	•	•	•	•	•
	S2	Steel braced frames	114		•	•		•		•			•	•	•						•	•			•	•	•	•			•	•	•	•		•	•		•	•
	S3	Steel light frames	125	•	•	•	•			•	•	•		•	•			•	•	•	•	•	•	•	•	•	•	•	•	•	•	•		•	•	•		•	•	•

Table A.4: Building material typology in District 4 (EMI 2022), where the row and column of **N** refer to the number of building typologies present per barangay and per typology (across the city), respectively.

				District 4 (38 barangays)																																					
				Bagong Lipunan ng Crame	**Botocan**	**Central**	**Damayang Lagi**	**Don Manuel**	**Doña Aurora**	**Doña Imelda**	**Doña Josefa**	**Horseshoe**	**Immaculate Concepcion**	**Kalusugan**	**Kamuning**	**Kaunlaran**	**Kristong Hari**	**Krus na Ligas**	**Laging Handa**	**Malaya**	**Mariana**	**Obrero**	**Old Capitol Site**	**Paligsahan**	**Pinagkaisahan**	**Pinyahan**	**Roxas**	**Sacred Heart**	**San Isidro**	**San Martin de Porres**	**San Vicente**	**Santol**	**Sikatuna Village**	**South Triangle**	**Sto. Niño**	**Tatalon**	**Teachers Village East**	**Teachers Village West**	**U. P. Campus**	**U. P. Village**	**Valencia**
Material	**Symbol**	**Description**	**N**	15	14	14	14	13	14	15	13	15	14	13	15	15	14	13	14	14	15	14	12	15	14	15	14	15	14	15	14	14	14	15	14	15	15	15	15	15	15
	W1W3	Wooden light-frame (small)	142	•	•	•	•	•	•	•	•	•	•	•	•	•	•	•	•	•	•	•	•	•	•	•	•	•	•	•	•	•	•	•	•	•	•	•	•	•	•
Wood	**W2**	Wooden light-frame (large)	142	•	•	•	•	•	•	•	•	•	•	•	•	•	•	•	•	•	•	•	•	•	•	•	•	•	•	•	•	•	•	•	•	•	•	•	•	•	•
	N	Makeshift or informal	141	•	•	•	•	•	•	•	•	•	•		•	•	•	•	•	•	•	•	•	•	•	•	•	•	•	•	•	•	•	•	•	•	•	•	•	•	•
	CHBMWS	Concrete hollow block	142	•	•	•	•	•	•	•	•	•	•	•	•	•	•	•	•	•	•	•	•	•	•	•	•	•	•	•	•	•	•	•	•	•	•	•	•	•	•
Masonry	**URA**	Unreinforced adobe walls	138	•	•	•	•	•	•	•	•	•	•	•	•	•	•	•	•	•	•	•		•	•	•	•	•	•	•	•	•	•	•	•	•	•	•	•	•	•
	URM	Unreinforced masonry walls	140	•	•	•	•	•	•	•	•	•	•	•	•	•	•	•	•	•	•	•		•	•	•	•	•	•	•	•	•	•	•	•	•	•	•	•	•	•
	RM2	Reinforced masonry walls with diaphragms	80	•					•	•		•		•	•	•					•			•	•	•	•	•		•	•	•		•		•	•	•	•	•	•
	CWS	Concrete with steel	142	•	•	•	•	•	•	•	•	•	•	•	•	•	•	•	•	•	•	•	•	•	•	•	•	•	•	•	•	•	•	•	•	•	•	•	•	•	•
	C1	Reinforced concrete moment frame	142	•	•	•	•	•	•	•	•	•	•	•	•	•	•	•	•	•	•	•	•	•	•	•	•	•	•	•	•	•	•	•	•	•	•	•	•	•	•
Concrete	**C2**	Reinforced concrete shear wall	142	•	•	•	•	•	•	•	•	•	•	•	•	•	•	•	•	•	•	•	•	•	•	•	•	•	•	•	•	•	•	•	•	•	•	•	•	•	•
	C4	Concrete shear walls and frames	142	•	•	•	•	•	•	•	•	•	•	•	•	•	•	•	•	•	•	•	•	•	•	•	•	•	•	•	•	•	•	•	•	•	•	•	•	•	•
	PC2	Precast concrete frames with shear walls	142	•	•	•	•	•	•	•	•	•	•	•	•	•	•	•	•	•	•	•	•	•	•	•	•	•	•	•	•	•	•	•	•	•	•	•	•	•	•
	S1	Steel moment frames	142	•	•	•	•	•	•	•	•	•	•	•	•	•	•	•	•	•	•	•	•	•	•	•	•	•	•	•	•	•	•	•	•	•	•	•	•	•	•
Steel	**S2**	Steel braced frames	114	•	•	•	•	•		•	•	•	•	•	•	•	•		•	•	•	•	•	•	•	•		•	•	•		•	•	•	•	•	•	•	•	•	•
	S3	Steel light frames	125	•	•	•	•		•	•		•	•		•	•	•	•	•	•	•	•	•	•		•	•	•	•	•	•		•	•	•	•	•	•	•	•	•